ACS OMEGA

Open Access

http://pubs.acs.org/journal/acsodf

Article

Design-of-Experiment-Assisted Fabrication of Biodegradable Polymeric Nanoparticles: In Vitro Characterization, Biological Activity, and In Vivo Assessment

Mushtaq Ahmad Mir, Md Habban Akhter, Obaid Afzal,* Safia Obaidur Rab, Abdulmalik S. A. Altamimi, Manal A. Alossaimi, Shehla Nasar Mir Najib Ullah, Mariusz Jaremko, Abdul-Hamid Emwas, Sarfaraz Ahmad, Nawazish Alam, and Md Sajid Ali

Cite This: *ACS Omega* 2023, 8, 38806−38821

Read Online

ACCESS | Metrics & More | Article Recommendations

ABSTRACT: Berberine (BER) is an alkaloid obtained from berberis plant having broad biological activities including anticancer. BER-encapsulated alginate (ALG)/chitosan (CHS) nanoparticles (BER−ALG/CHS-NPs) were developed for long-acting improved treatment in breast cancer. The surface of the NPs was activated by a conjugation reaction, and thereafter, the BER−ALG/CHS-NP surface was grafted with folic acid (BER−ALG/CHS-NPs−F) for specific targeting in breast cancer. BER−ALG/CHS-NPs−F was optimized by applying the Box−Behnken design using Expert design software. Moreover, formulations are extensively evaluated in vitro for biopharmaceutical performances and tested for cell viability, cellular uptake, and antioxidant activity. The comparative pharmacokinetic study of formulation and free BER was carried out in animals for estimation of bioavailability. The particle size recorded for the diluted sample using a Malvern Zetasizer was 240 ± 5.6 nm. The ζ-potential and the predicted % entrapment efficiency versus (vs) observed were +18 mV and 83.25 ± 2.3% vs 85 ± 3.5%. The high % drug release from the NPs was recorded. The analytical studies executed using infrared spectroscopy, differential scanning calorimetry, and X-ray diffraction expressed safe combinations of the components in the formulation and physical state of the drug revealed to be amorphous in the formulation. Cytotoxicity testing demonstrated that the formulation effectively lowered the cell viability and IC_{50} of the tested cell line in comparison to a raw drug. The cellular uptake of BER−ALG/CHS-NPs−F was 5.5-fold higher than that of BER−suspension. The antioxidant capacities of BER−ALG/CHS-NPs−F vs BER−suspension by the DPPH assay were measured to be 62.3 ± 2.5% vs 30 ± 6%, indicating good radical scavenging power of folate-conjugated NPs. The developed formulation showed a 4.4-fold improved oral bioavailability compared to BER−suspension. The hemolytic assay intimated <2% destruction of erythrocytes by the developed formulation. The observed experimental characterization results such as cytotoxicity, cellular uptake, antioxidant activity, and improved absorption suggested the effectiveness of BER−ALG/CHS-NPs−F toward breast cancer.

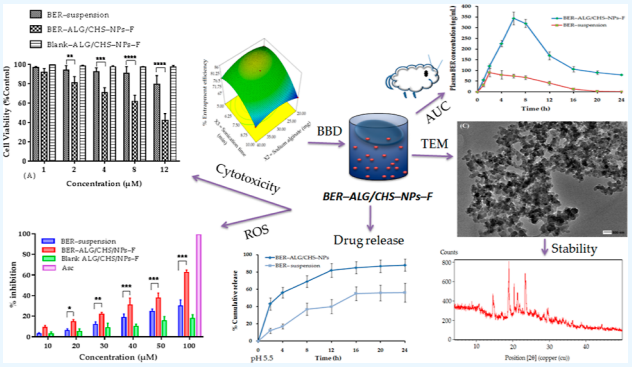

1. INTRODUCTION

Breast cancer is a progressive and malignant tumor, causing mortality worldwide, despite the recent advancement and progress in cancer treatments. The incidence rate of this cancer among women is highest compared to other types of cancers. As per 2022 new estimates, around 287,850 cases of breast cancer have been diagnosed, and there are 43,250 cases of estimated death. The incidence rate of breast cancer in female accounts for nearly one-third.[1] Conventional treatment strategies such as surgery, chemotherapy, and radiotherapy have been conflated for several decades aiming to treat cancer cell mass. Chemotherapy is still largely used in cancer treatment; however, it is usually not enough alone in therapeutic strategies and complete cure of the disease. Therefore, more studies are increasingly seeking accuracy in therapeutic modules and preventing drug resistance. Cancer therapy is probably complicated due to resistance development toward chemotherapy, causing a sub-therapeutic effect in patients.[2] In addition, it may cause life-threatening toxicity due to nonselective, off-target drug release

Received: February 20, 2023
Accepted: April 21, 2023
Published: October 11, 2023

and multidrug resistance.[3] The aqueous-state drug solubility, dissolution, and poor absorption of chemotherapeutic agents are challenging tasks. To surmount the challenges faced with chemotherapy, there is a compelling indigence to develop a drug delivery platform that is safe and efficacious in treating the disease but at the same time minimizing severe untoward effects to the healthy cells. Moreover, chemotherapy in combination with radiotherapy is preferred in suppressing tumor growth.[4]

Nanotechnology offers a novel platform to process and develop nanoparticles (NPs) of desired size and shape of multifunctionality in an interdisciplinary area of science and their application in medicine.[5] The NP drug delivery system trending toward a successful development of a drug product achieved large popularity toward therapeutic effects due to more accurate, specific, and targeting capabilities and thus increased the drug concentration in the target area.[6] It has been established that the targeted drug delivery led to the development of a broad range of NP therapeutic systems applying different nanocarrier systems such as polymer-based, lipid-based, organic, metallic, dendrimer, carbon dots, and nanorods in cancer therapy.[7−14]

The tumor microenvironment is disorganized, has a leaky vasculature, and can receive drug through the passive targeting mode mediated via the enhanced permeability and retention mechanism or targeted drug delivery for specific drug targeting. The passive targeting approach, however, restricts the potential drug delivery to the target due to the variable interstitial pressure and growth of angiogenic factors, and this could be accosted in a preclinical study. The growing interstitial fluid pressure in tumor loci and angiogenic factors and the reduced transcapillary diffusion due to high interstitial pressure in the microenvironment restrict the warehouse campaign, resulting in pathetic drug release.[15] The targeting capabilities of nanocarriers are further limited by encasing of protein molecules or biocorona in the biological fluid. Moreover, the tumor microenvironment bears large fenestration, an endothelial pore, and a disoriented microvasculature, helping to infiltrate and accrue majority of therapeutics in the neighboring cells without causing harm to the normal cells.[16,17] Polysaccharides have been investigated as a new class of drugs[18] and drug carriers[19] for many diseases including cancer, viral infections, and neurological disorders.[20] Chitosan (CHS) is an approved natural polysaccharide composed of glucosamine and *N*-acetyl glucosamine derived from crab shells and the fungal cell wall. CHS bears a cationic surface charge, basic in nature and having mucoadhesive properties, obtained from chitin. It is a deacetylated product of chitin obtained after purification and alkalization processes.[21] It constitutes a stable structure with alginic acid to better encapsulate drugs and prevent their loss through degradation. CHS is a penetration promoter for drugs or active moieties through a paracellular or transcellular route. The positive charge on CHS interacts actively with the negatively charged surface of the mucus. The multifunctional groups on CHS molecules (e.g., −OH, −COOH, and $-NH_2$) are an ideal target site for surface tuning, which can enhance the drug dissolution and bioavailability of lipophilic drugs.[22]

Alginate (ALG) is composed of two monomer units of α-L-guluronic acid (G-block) and β-D-mannuronic acid (M-block) of a linear polysaccharide derived from seaweed. The G-block having high ionic affinity with divalent metal ions like a calcium ion (Ca^{2+}) or polyvalent cations forms an insoluble three-dimensional (3D) network. An "egg box model" with a cross-linked structure resulted via the ionic interaction of ALG with divalent ions. The 3D network facilitates the preparation of a wide range of drug delivery systems including NPs for release of drugs, proteins, and pharmaceuticals.[23] It possesses gelling property, mucoadhesive nature, and natural compatibility with the cell components in the biological system and can be promisingly useful as a drug delivery carrier in bioengineering and medical applications.[24] The ionotropic gelation involves an electrostatic interaction between CHS and ALG, resulting in the formation of CHS−ALG NPs in an aqueous environment. In ionotropic gelation, the ALG molecule undergoes interfacial polymerization in the G-block of the guluronic residue, leading to formation of NPs.[25]

The application of natural products is increasing day-to-day due to favorable characteristics and biofriendly uses and led to a dramatic change in the development of natural products. The NP-based drug delivery opens up a novel platform to expedite therapy in particular ailments with a precise and specific way. To address the challenging diseases through manipulating the NP feature may result in the development of a smart therapeutic system encasing drugs, biological agents, and chemotherapeutic agents. A wide range of biological molecules from herbal origin have been implicated in different biological activities using nanodrug delivery platforms.[26−32] Berberine (BER) regresses cell invasion, metastasis through suppressing the PI3K/Akt signaling pathway, and downregulation of protein expression associated with cancer metastasis. It reduces cell proliferation by different molecular mechanisms including cell cycle modulation, interaction with micro-RNAs, and inhibition of telomerase activity. An autophagic suppressor is another mechanism responsible for curbing autophagosomes in an adverse drug reaction-related breast cancer mediated via regulating PTEN, protein LC3II, and p62 accumulation, resulting in inhibition of cell proliferation and suppression of doxorubicin resistance.[33] BER also exerts anti-inflammatory and antioxidant properties and regulates the tumor microenvironment.[34] In breast cancer, BER apprehends cells at the beginning of the cell cycle and may also sensitize the cancer cells toward chemotherapy.[35] It was also reported that BER acts via oppressing the mRNA levels of a chemokine receptor and thus reduces MCF-7 cell migration.[36] BER has been reported to have various biological activities including antimicrobial,[37] anti-inflammatory,[38] antidiabetic,[39] and anticancer.[40]

2. MATERIALS AND METHODS

2.1. Reagents. Chitosan (Mol. wt. 50−190 KDa, 85% deacetylation) and sodium alginate (Mol. wt. 75−100 KDa) were received from Cisco Research Laboratories (SRL). BER was purchased from TCI Chemicals Pvt. Ltd., India. The chemicals, reagents, and solvents employed in this study were of analytical grade. The breast cancer cell line was obtained from the National Centre for Cell Science (Pune, India). The Dulbecco's medium supplied with an antibiotic (100 mg/mL), fetal bovine serum (10%), and penicillin (100 unit/mL) were used to keep the culture cells viable under controlled temperature and humidity.

2.2. Design Optimization. The cost-effective and most efficient optimization tool such as Design-Expert software (version 10; Stat Ease Inc., Minneapolis, MN, USA) of the Box−Behnken design was used at three levels of low, intermediate, and high (−1, 0, and +1), two factors, for finalizing the desired formulation, BER−ALG/CHS-NPs−F.[27,31] The finalized list of independent variables as per the trial and error basis marked with levels is aligned in Table 1. The screened components of

https://doi.org/10.1021/acsomega.3c01153
ACS Omega 2023, 8, 38806−38821

Table 1. Different Levels of Factors and Their Responses as Low, Medium, and High in the Optimization of BER−ALG/CHS-NPs−F in the Box−Behnken Design

	levels used		
factors	low (−1)	medium (0)	high (+1)
X1: chitosan (mg)	10	20	30
X2: sodium alginate (mg)	20	30	40
X3: sonication time (min)	5	7.5	10
responses		goal	
Y1: particle size (nm)		minimize	
Y3: EE (%)		maximize	

the study such as CHS, ALG, and sonication time having important roles in determining the fate of the formulation were chosen as independent variables. The effect of independent variables was noted on responses such as particle size and entrapment efficiency (EE). The software-generated different experimental runs comprising the varying percentage of independent variables were performed in a successive manner in optimizing the formulation (Table 2). Statistical analysis was

Table 2. In Vitro Assessed Parameters and Their Output of Formulations of Runs (1−15) for Responses in the Optimization Process of BER−ALG/CHS-NPs−F[a]

	factors			responses	
experimental run	X1, mg	X2, mg	X3, min	Y1, nm	Y2, %
1	0	−1	10	278	82.0
2	+1	0	10	297	88.0
3	0	0	7.5	287	80.0
4	+1	0	5.0	277	91.0
5	−1	+1	7.5	269	82.0
6	−1	0	5.0	281	87.0
7	+1	+1	7.5	299	80.0
8	−1	−1	7.5	268	69.0
9	0	−1	5.0	302	89.0
10	0	+1	5.0	301	90.0
11	0	0	7.5	294	78.0
12	+1	−1	7.5	216	77.0
13	−1	0	10	213	86.0
14	0	0	7.5	290	78.8
15	0	+1	10	272	93.0

[a]X1: CHS, mg, X2: sodium ALG, mg, X3: sonication time, min, Y1: particle size, nm, and Y2: % EE.

performed using one-way ANOVA to obtain the model summary analysis, which ensured good fit with optimized preparation. The optimum composition of BER−ALG/CHS-NPs−F was generated using the point prediction technique, keeping the criteria of particle size (minimize) and EE (maximize).

2.3. Preparation of the Folate Conjugate (BER−ALG/CHS-NPs−F). The prepared NPs of weight 10 mg were transferred to a 1 mL phosphate buffer saline (PBS) solution and magnetically stirred; concomitantly, 20 mg/mL EDC in deionized water was slowly added to the NP dispersion and magnetically stirred thoroughly. Separately, sulfo-NHS, 5 mg/mL, was dissolved in a physiological buffer, pH 7.4, and injected in the above-mentioned solution under magnetic stirring. The treated NP dispersion was kept overnight in a biological shaker for complete surface activation. Further, the surface-activated NPs were centrifuged at 14,000*g*, the aliquot was discarded, and the residual NPs were washed using PBS in triplicate (n = 3), dried, and redispersed in 500 μL of PBS. Folic acid (10 mg) was stirred in 5 mL of sodium chloride, integrated into polymeric dispersion, and magnetically stirred continuously in a biological shaker maintained in the dark for 24 h for surface grafting of folic acid onto the NPs. The folate-grafted NP dispersion was centrifuged at 10,000×*g* for 25 min, the aliquots were removed, and the NPs were washed, freeze-dried to powder, and stored temporarily for characterization.[29]

2.4. Characterization. *2.4.1. Particle Size Measurement.* The particle size was determined using a Zetasizer (Hitachi, H-7500). For particle size analysis, the formulation was diluted to 100-fold using distilled water, mixed well, and observed at a scattering angle of 25 °C at room temperature.

2.4.2. Entrapment Efficiency. The amount of BER encapsulated in the formulation was investigated after centrifugation. The supernatant was pulled out using a micropipette, and the drug concentration was estimated with the help of a UV−visible spectrophotometer. The formula for calculation of % DL is as follows

$$\%\ \text{EE} = \text{the total drug taken} - \text{the drug in the supernatan}$$
$$\text{t/the total drug taken} \times 100 \quad (1)$$

2.4.3. Drug Loading. The total quantity of the drug encapsulated per unit weight of NPs indicated drug loading. It is determined by centrifugation of 1.5 mL of NPs and estimating the concentration of the free drug using a UV spectrophotometer. The formula for calculation of % DL is as follows

$$\%\ \text{DL} = \text{drug} - \text{entrapped NPs/total NP weight} \times 100 \quad (2)$$

2.4.4. Thermal Scanning. A differential scanning calorimetry (DSC) instrument was used to check the melting point of the drug, and drug−excipient interaction. For the thermal scanning study, ∼5 mg of the samples were placed in DSC pans, and heated continuously to 285 °C under dry nitrogen gas.

2.4.5. Fourier Transform Infrared. BER and different excipients used in the formulation were assessed by a Fourier transform infrared (FTIR) spectrometer (Bruker Corporation, Billerica, MA, USA). For spectral analysis, 3−5 mg of BER, CHS, and sodium ALG were held on the path of the incident light beam scanned in the wavenumber range of 400−3500 cm^{-1}, and their spectrum was recorded and analyzed.

2.4.6. X-ray Diffraction Study. X-ray diffraction (XRD) studies of the excipients (CHS and sodium ALG), plain drug, and formulation were carried out with a simple phase analysis (Rigaku Ultima IV) working under a voltage of 40 kV, a current of 30 mA, and a monochromatic light radiation of wavelength 1.5406 Å. The 2θ angle ranges from 10 to 80° under a scanning speed of 8°/min, and the detector used was a scintillation counter.

2.5. Drug Release Study. The drug release from the developed formulation and drug suspension was studied in PBS of pH 7.4 and pH 5.5 in a dialysis membrane. The membrane was previously charged in a dissolution medium. The measured amount of formulation, BER−ALG/CHS-NPs−F, and drug dispersion with the same dose (10 mg) was entrapped in a tightly packed dialysis membrane containing 100 mL of PBS, dipped in a buffer medium, and continuously stirred at 100 rpm under a controlled temperature of 37 ± 0.5 °C.[36] At the last point of the study, 0.1 mL of the sample was withdrawn at prefixed intervals (0, 2, 4, 8, 12, 16, 20, and 24 h), and the same

https://doi.org/10.1021/acsomega.3c01153
ACS Omega 2023, 8, 38806−38821

volume was substituted with the fresh buffer medium. The sample was analyzed for determining the concentration of BER using a UV spectrophotometer and the percentage of drug release. The drug release data obtained was fitted into various kinetic models. The best best-fitted model was then analyzed with the model of good fit using a graphical method. Further, the drug release mechanism equates to Fickian diffusion, when the exponent value $n \leq 0.5$. On the other hand, when $0.5 < n < 1$, the drug diffusion from the polymer matrix relates to an anomalous, non-Fickian drug diffusion. Further, $n = 1$ relates to a non-Fickian, case II (relaxational) transport or zero-order release kinetics and $n > 1$ relates to a supercase II transport.[29,41]

2.6. Ex Vivo Permeation Study. The extraneous material, adhered particle, or cell debris from the intestine was cleaned in buffer solution and prepared for the study.[42,43] The formulation, BER−ALG/CHS-NPs−F and BER−suspension, bearing 10 mg of the drug was transferred in different intestinal sacs, and both the terminal ends were well ligated. Now, the filled intestinal sac was plunged in a receiver containing 100 mL of physiological buffer, which is well aerated at a constant temperature, 37 ± 0.5 °C, and the sample was continuously agitated to the entire the experiment. At different time points, 500 μL of the sample was drawn, and the same medium volume was put back in the receiver with the buffer solution. The collected samples at various intervals (0, 4, 8, 12, 16, 20, and 24) were quantified by a UV spectrophotometer at 210 nm. The amounts of BER from BER−ALG/CHS-NPs−F permeated through the intestinal membrane were compared with the BER−suspension at different intervals of time, and the drug-permeated amount was determined. The apparent permeability coefficient (P_{app}) is determined by the following equation

$$P_{app}\ (\mathrm{cm/s}) = \mathrm{d}Q/\mathrm{d}t \times A \times C_o \quad (3)$$

where $\mathrm{d}Q/\mathrm{d}t$ is the permeation flux of the analyte across the barrier, A is the surface area, and C_0 is the initial concentration of the drug in the donor compartment.

2.7. Cytotoxic Assay. To investigate the cytotoxic effect of the developed dosage form, BER−ALG/CHS-NPs−F and BER−suspension were incubated with the MCF-7 cell line in an increasing drug concentration. Five thousand cells were seeded in a 96-well plate, and the plate was incubated for 24 h at a temperature of 37 °C. After completion of the time, the culture medium was well disposed off from the plate, and an increasing concentration of the formulation and drug dispersion (1−12 μM) was received, each having the same dose. The plate was incubated for 24 and 48 h immediately after transferring the drug concentration at a temperature of 37 °C. After the incubation period, the culture medium was discarded from each plate and replaced with 10 μL of the MTT reagent and again kept in the incubator for 4 h. Further, the supernatant was blown off from the plate, and 100 μL of dimethyl sulfoxide was incorporated into it. The absorbance was measured at 570 nm wavelength and analyzed on a microplate reader (Bio-Rad, Hercules, CA, USA).[31] The cells were considered 100% viable in the untreated group. The IC_{50} concentration (50% of cells remained viable) was determined for both drug dispersion and formulation. The % cell viability was determined by using the following equation

$$\%\ \text{Cell viability} = \text{sample OD}/\text{controlled OD} \times 100 \quad (4)$$

2.8. Cellular Uptake Study. The in vitro cell viability study was further confirmed by cellular uptake of the folate-modified formulation, BER−ALG/CHS-NPs−F, and BER−suspension in a breast cancer cell line. The six-well plates were incubated with 1×10^6 cells at 37 °C for 1 day. Thereafter, equivalent concentration (15 μg/mL) each of BER−ALG/CHS-NPs−F and BER−suspension was transferred into the six-well plate and incubated for 4 h. The wells were subjected to buffer wash, sterile water was used to lyse the cells, and drug was extracted from the cells using an organic solvent leaving behind the protein precipitate. The extracted drug was centrifuged at 12,000 rpm, and a clear aliquot was removed, filtered using 0.45 μ size membrane filters, and analyzed by injecting into a high-performance liquid chromatography (HPLC) column.

2.9. In Vivo Evaluation. In vivo pharmacokinetic experiments were designed and conducted according to the ethical guidelines approved by the Institutional Animal Ethics Committee (IAEC), DIT University, India (ref no. DITU/IAEC/22/01-05). For the estimation of a pharmacokinetic parameter, a single dose was administered into male Wistar rats divided in a randomized way into two groups from control group animals (untreated). One group received the formulation, BER−ALG/CHS-NPs−F, at a dose of 80 mg/kg, and the other group received BER−suspension of the same dose orally. After dosing, 150 μL of blood has been withdrawn from the animal's tail vein in heparinized Eppendorf tubes at predefined intervals (0, 1, 2, 4, 8, 12, 16, 20, and 24 h). The samples further processed for extracting plasma, using acetonitrile and ethyl acetate, vortexed, and centrifuged 3000 rpm for 15 min. The supernatant part of the sample was separated and kept at −20 °C for analysis. The sample aliquot was recovered and dried, and the received residue was dispersed in 200 μL of DMSO and analyzed for drug content using HPLC. Using PK Solution 2.0 software, a noncompartmental pharmacokinetic data analysis was employed to determine the pharmacokinetic parameters.

2.10. Hemolysis Assay. This assay as performed using citrate-buffered whole blood brings in contact with the fabricated polymeric formulation of BER. The formulation was diluted two times in physiological saline of 0.9% w/v. The citrated blood was centrifuged at 3000 rpm for 15 min, the supernatant removed was mixed with the diluted formulation in a ratio of 2:1, and the mixture was incubated for 1 h at a physiological temperature. The other part of the whole blood was mixed with deionized water (complete hemolysis) and saline in a ratio of 1:1.25 to make it as a positive and negative control. Post-incubation time, the samples were obtained and centrifuged at 3000 rpm for 15 min. Thereafter, the clear aliquot was taken out, the absorbance of each sample was measured at 540 nm using a UV−visible spectrophotometer, and the hemoglobin quantity released due to RBC damage was recorded. The hemolytic index or percentage hemolysis was calculated using the formulation.

$$\%\ \text{Hemolysis} = \frac{\text{Abs TS} - \text{Abs NC}}{\text{Abs PC} - \text{Abs NC}} \times 100 \quad (5)$$

where "Abs TS" indicates the absorbance measured for the test sample, "Abs NC" indicates the absorbance of the negative control, and "Abs PC" indicates the absorbance measured for the positive control.

2.11. DPPH Radical Scavenging Assay. The radical scavenging property of BER−ALG/CHS-NPs−F and BER−suspension was investigated by diluting in ethanol following DPPH assay by modification in the work reported.[44] Ascorbic acid was used as a standard for comparing the antioxidant property. The assay relies on the radical scavenging action of the antioxidant sample when reacted with the DPPH reagent. For performing the antioxidant study using DPPH assay, a standard

https://doi.org/10.1021/acsomega.3c01153
ACS Omega 2023, 8, 38806−38821

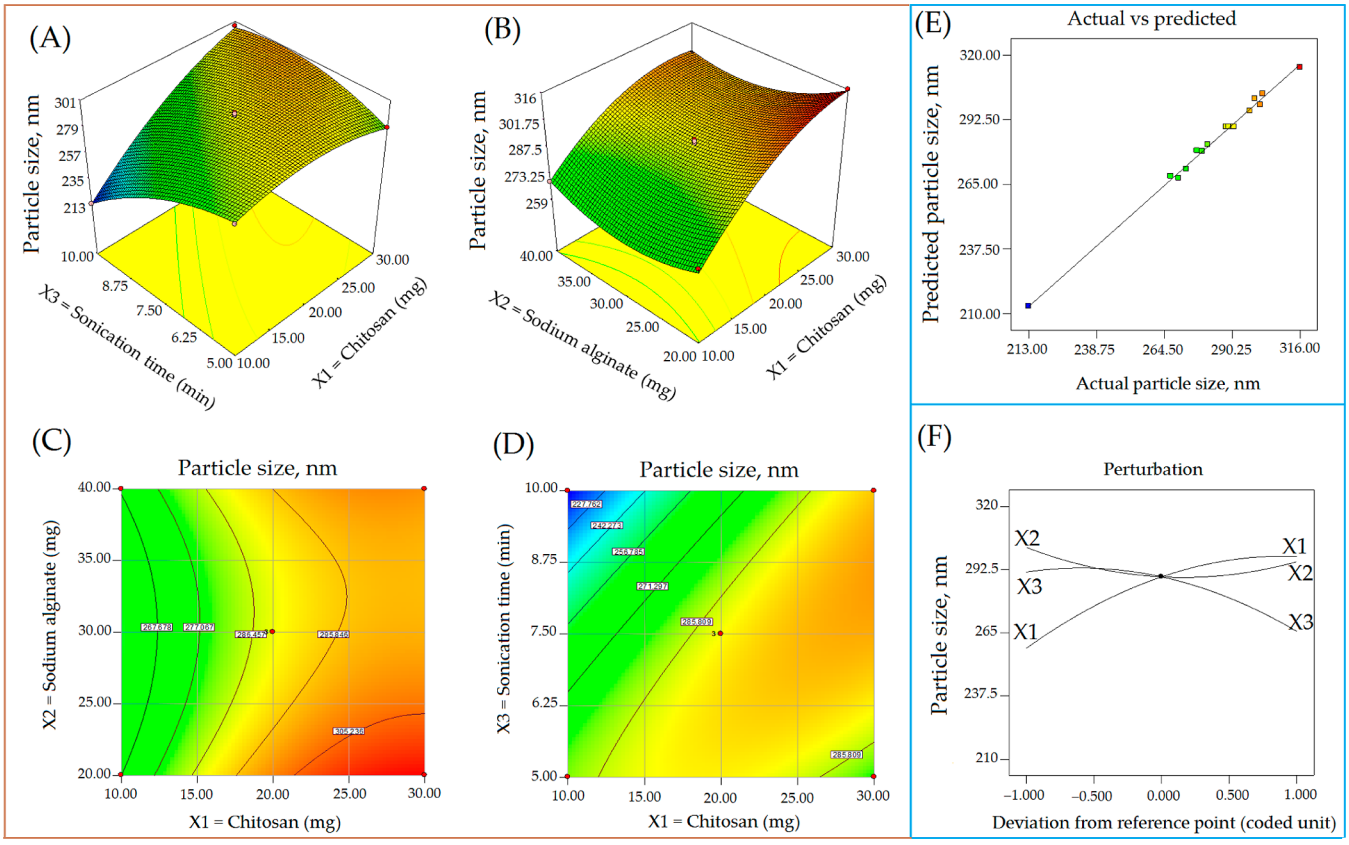

Figure 1. 3D response surface plot (A,B) and contour plot (C,D) of particle size. Actual vs predicted particle size (nm) (E), perturbation curve (F) expressing the impact of process variables, X1 = CHS (mg), X2 = sodium ALG (mg), and X3 = sonication (min) on the particle size of BER−ALG/CHS-NPs−F.

stock solution of formulation and drug suspension in DMSO were prepared with a final concentration of 10 mg/mL. The DPPH reagent (500 μL, 0.04% w/v) was added to the samples, mixed well, and kept in the dark at room temperature for some time. The violet color of the sample is lost to colorless as the sample reacted with the DPPH reagent due to the antioxidant property. Ethanol was used in the preparation of a blank mixture . The absorption of samples such as the formulation and drug suspension was investigated using UV−visible spectroscopy at a λ_{max} value of 517 nm. The antioxidant power of the formulation and drug suspension was compared as % inhibition. The radical scavenging power of the formulation was also compared with the standard ascorbic acid. The graph was plotted between % radical scavenging capacities vs concentration of samples. The IC_{50} value was determined by data interpolation and compared with the standard. The experiment was performed three times (n = 3). It is calculated by using the following equation.

$$\%\ \text{DPPH radical inhibition} = C_o - C_1/C_o \times 100 \quad (6)$$

where C_o is the blank sample absorbance and C_1 is the sample absorbance.

2.12. Stability of the Formulation. The optimum formulation was subjected to stability at room temperature, 25 ± 2 °C, 60% RH for a period of 90 days.[45,46] The samples were placed inside the stability testing apparatus (Hicon Engineering Pvt. Ltd. India). The formulation was analyzed at a predefined time period in a 1 month interval to inspect the changes in the physicochemical properties of the formulation, especially particle size, polydispersity index (PDI), and % EE. The experiments were repeated thrice to get the reproducible results (n = 3).

2.13. Data Analysis. The analysis for statistical differences in the treatment groups was executed using ANOVA, followed by Tukey-Kramer analysis using GraphPad prism version 7. The data obtained here are represented by mean ± standard deviation (n = 3). The statistical differences among the groups were considered significant when $p < 0.05$.

3. RESULTS AND DISCUSSION

3.1. Optimization of the Formulation. BER−ALG/CHS-NPs−F was prepared and optimized using the statistical design 3^3-Box−Behnken. The variables played an important role in the optimization process and were used in three levels: low (−1), medium (0), and high (+1). The concentrations of variables under each level projected by software in various proportions were experimented, and their impact on responses were studied. The levels (−1, 0, and +1) of variables were picked out based on trial and error basis on preliminary investigation (Table 1). Figures 1 and 2 depict the counterplots in the two-dimensional mode and the response surface morphology plots in the 3D mode, which delineates different variable effects on responses of designed formulations. The highest value of coefficient of correlation (R^2) ∼1 was found for the quadratic model and considered as the best best-fitted model for ascertaining the effect of input attributes on the responses. Among the various models, quadratic model was the best-fitted model that established the individual, interaction, and quadratic impact on the responses. The regression analysis of various responses

https://doi.org/10.1021/acsomega.3c01153
ACS Omega 2023, 8, 38806−38821

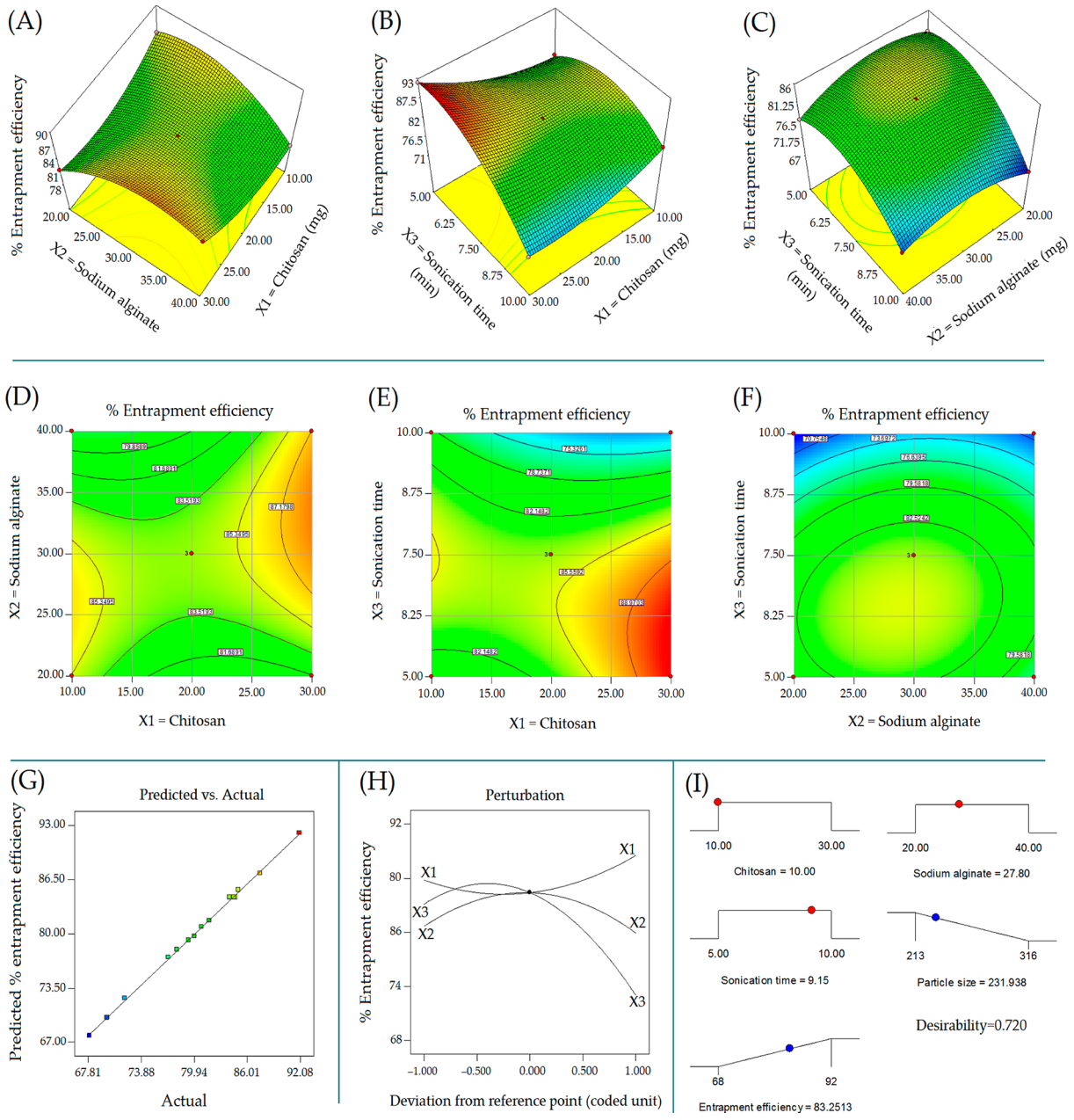

Figure 2. 3D response surface plot (A−C), contour plot (D−F), actual vs predicted particle size (E), and perturbation curve (F) expressing the impact of process variables, X1 = CHS (mg), X2 = sodium ALG (mg), and X3 = sonication (min) on Y1 (particle size, nm) of BER−ALG/CHS-NPs−F. Linear plot showing predicted vs actual EE (G). Ramps plot showing the numerically optimized level of input attributes (I), red dot indicates the optimized level, while blue dot indicates the predicted particle size.

Table 3. Summarized Regression-Analyzed Experimental Results of Responses, Particle Size, and % EE

model	R^2	adjusted R^2	predicted R^2	SD	CV %	PRESS	desirability	remark
response: particle size						519.50	0.85	
quadratic	0.9954	0.9872	0.1340	2.68	0.95			suggested
2FI	0.8305	0.7034	0.1669	4.39				
linear	0.5879	0.4755	0.9348	7.50				
cubic	0.9994	0.9958		1.53				aliased
response: % EE						7.43		
quadratic	0.9989	0.9968	0.9878	0.37	0.46			suggested
2FI	0.5986	0.2975	−0.7890	5.52				
linear	0.3639	0.1905	−0.2792	5.93				
cubic	0.9996	0.9970		0.36				aliased

https://doi.org/10.1021/acsomega.3c01153
ACS Omega 2023, 8, 38806−38821

for the data fitting into the distinguished model is expressed in Table 3.

3.1.1. Effect of X1, X2, and X3 on Particles Size. The impact on particle size is illustrated by the following equation

$$\text{Particle size} = +289.33 + 20.00 \times X1 - 3.13 \times B - 12.88 \times C - 3.50 \times A \times B + 21.50 \times A \times C - 11.04A^2 + 9.71 \times B^2 - 10.79 \times C^2 \quad (7)$$

The particle size plays a pivotal role in improved cellular uptake and absorption-active molecules from nanocarriers mediated via cytosolic release of therapeutics into the cancer cells. The above quadratic equation for particle size, 3D response surface plot (Figure 1A,B), contour plot (Figure 1C,D), actual vs predicted particle size (Figure 1E), and perturbation curve (Figure 1F), illustrating the considerable influence of process parameters in the particle size.

As shown in Table 2, the particle sizes of the folate-conjugated formulation, BER−ALG/CHS-NPs−F, incurred in the ranges 213−302 nm, indicating narrow distribution of particle size in the formulation. The polymer, CHS, had positive impact on particle size; conversely, sodium ALG and sonication had negative influence on particle size. The selected process variable had a significant impact on particle size as indicated by ANOVA of particles size. At low CHS concentration (10 mg), the least particle size incurred 213 nm, and the highest particle size obtained 302 nm at 20 mg of CHS concentration may be due to the low sonication time and impact of other variables. Still at the highest CHS concentrate, 30 mg led to 299 nm particle size. Increasing CHS concentration progressively raised the particle size. Sodium ALG had less negative impact on particle size as illustrated by the above quadratic equation of particle size. At low concentration of sodium ALG, the particle size obtained was 302 nm, as can be seen in the formulation run 9, while increasing ALG concentration to 40 mg led to reduced particle size as can be seen in the formulation run 15. Sonication had negative impact on particle size. Sonicating CHS/ALG NPs for 5 min produced a particle of size of 302 nm (run 9). Increasing sonication time to 10 min led to reduced particle size to 213 nm as given in Table 2 (run 13). Sonication generally produced an ultraviolet wave causing size reduction in the nanoparticulate system. Apart from these, the molecular weight, percentage deacetylation, and percentage of ALG/CHS in the polymeric core may influence the resulting particle size.[47] CHS−ALG interaction protects therapeutics/biomolecules from degradation mediated via enzymatic, hydrolysis, and oxidation in the surrounding environment and thus assures effective and drug delivery to the target.[48] The CHS−ALG NPs prolonged the contact with the epithelia of mucosal cell lining and help to penetrate the drug through cellular tight junction and thus enhance drug absorption.[49] The interactive effect of CHS and ALG was less negative on the particle size, while the interactive impact of CHS and sonication time was positive.

3.1.2. Impact of X1, X2, and X3 on % EE. The influence of process variables such as X1, X2, and X3 on the % EE is shown by the following equation

$$\%\ \text{EE} = +84.40 + 1.36 \times A - 0.38 \times B - 5.06 \times C + 3.20 \times A \times B - 4.83 \times A \times C + 1.45 \times B \times C + 2.76 \times A^2 - 4.11 \times B^2 - 6.34 \times C^2 \quad (8)$$

The higher the EE, the better will be the therapeutic efficacy of the drug delivery system. The EE of BER−ALG/CHS-NPs−F ranges in between 69 and 93% as indicated in Table 2. ANOVA of the response surface quadratic revealed significant influence of X1, X2, and X3 on % EE. The ANOVA results for particle size and % EE fitting to the quadratic model are shown in Table 4.

Table 4. ANOVA for Response Surface of Particle Size and % EE and Lack of Fit for the Best-Fitted Quadratic Model for Optimizing BER−ALG/CHS-NPs−F

		regression analysis	
model	source	particle size	% EE
quadratic	sum of square	7795.82	606.57
	Df	9	9
	mean square	866.20	67.40
	F-value	120.58	490.16
	p-value, prob > *F*	<0.0001	<0.0001
	inference	significant, suggested lack of fit	significant, suggested
quadratic	sum of square	31.25	0.43
	Df	3	3
	mean square	10.42	0.14
	F-value	4.46	1.10
	p-value, prob > *F*	0.1886	0.5097
	inference	insignificant, suggested	insignificant, suggested

The above quadratic equation for % EE expressed the individual, combined, and quadratic impact of formulation variables on % EE. Further, the impact of X1, X2, and X3 on % EE is shown in a 3D surface response surface plot [Figure 1A−C] and a contour plot [Figure 1D−F]. The actual particle size vs the predicted particle size linear curve (Figure 1E) and perturbation curve (Figure 1F) has conveyed the impact on % EE. CHS had positive impact on EE. Increasing polymer concentration increased the surface area to accommodate more drug as well as viscosity in the formulation bulk, thus reducing the drug leaking from the polymeric matrix.[50] The ALG concentration had less negative effect on % EE. The combining effect of ALG and CHS exerted positive on produced NPs was observed due to the electrostatic interaction between the ALG carboxyl and CHS amino groups, leading to the blenching and gel formation at acidic pH. At a low ALG concentration, 20 mg, the % entrapment was 89% as can be seen in run 9, while at 40 mg of ALG concentration, the % entrapment was reported to be 82%, as indicated in experimental run 5. The optimized formulation biopolymer generated consistent and homogeneous preparation. Similarly, the gel-forming tendency of the ALG/CHS complex may assist in improved EE with better drug holding capacity. Additionally, the cross-linker Ca^{2+} ion complex opposite to charged CHS precedes to improved drug entrapment in the nanocomposites.[51,52]

3.1.3. Analysis of the Optimized Formulation. The composition of the optimum formulation was obtained by applying the numerical optimization technique, keeping the

https://doi.org/10.1021/acsomega.3c01153
ACS Omega 2023, 8, 38806−38821

criteria of minimum particle size, PDI, and maximum % EE. The optimum formulation was analyzed with respect to various selected parameters experimentally, and the findings were in agreement with the predicted values. The value of desirability of the optimized formulation was 0.720, indicating that the prepared formulation was consistent and robust. The optimum concentration of the developed formulation, BER−ALG/CHS-NPs−F, has CHS, ALG, and sonication time in a proportion of 10 mg, 27.8 mg, and, 9.15 min, respectively. Comparing the predicted vs experimental value, the optimized formulation composition was varying as particle size 232 nm vs 240 ± 5.6 nm and % EE 83.25 ± 2.3% vs 85 ± 3.5%, respectively. The % drug loading in the optimized formulation reported to be 9.5 ± 1.2%. Some percentage error was reported while comparing the data obtained in theoretical and practical yield values, and these errors were in the acceptable limit (Y1 = 3.4% and Y2 = 2.1%) (Table 5). Further, the variation in the experimental value and

Table 5. Percentage Error in the Optimized Formulation (BER−ALG/CHS-NPs−F) Reported While Comparing the Experimental Value vs the Predicted Values[a]

	predicted value		experimental value		
factors (X1, X2, and X3) and optimized composition	Y1, nm	Y2, %	Y1, nm	Y2, %	†
X1 = 10 mg, X2 = 27.8 mg, and X3 = 9.15 min	232	83.25	240	85	Y1 = 3.4 and Y2 = 2.1

[a]X1: CHS, mg; X2: sodium ALG, mg; X3: sonication time, min; Y1: particle size, nm; and Y2: % EE.

predicted value was statistically not different ($p < 0.05$). In addition, surface charge on the particles determined +18 mV may be attributed to the cationic surface of CHS, which indicated the stability of the optimized formulation. The low value of PDI (0.201) confirmed homogeneous and uniform particle distribution.[53]

$$\text{Percentage error}(\dagger) = (\text{experimental} - \text{predicted})\text{value}/\text{predicted value} \times 100 \quad (9)$$

3.2. Characterization. *3.2.1. Particle Size, PDI, Charge Surface, and TEM.* The developed formulation optimally revealed a particle size of 240 ± 5.6 nm, a zeta potential of +18 mV, and a PDI of 0.201. The drug entrapment and drug loading were measured as 85 ± 3.5 and 9.5 ± 1.2%, respectively. The particle distribution was uniform, unimodel, and consistent. The low PDI (0.201) expressed a homogeneity and monodispersed system. The positive surface charge was confirmed on formulation BER−ALG/CHS-NPs by zeta potential measurement, and it was noted as +18 mV, suggesting that the positive surface charge was due to CHS. It can be explicated that the presence of protonated amino group in CHS led to stability to the nanocarrier system and portrayed the fate of NPs in the biological system.[54] The size distribution curve and the zeta potential of BER−ALG/CHS-NPs−F are shown in Figure 3A,B. Transmission electron microscopy (TEM) examination revealed that the particle size in preparation was in nanometer (nm) scale, uniform, consistent, scattered, and stable (Figure 3C).

3.2.2. Differential Scanning Calorimetry. The physical state of the processed drug in the nanocarrier is highly important in the drug delivery approach. DSC expressed the physical state of the drug in the nanocarrier and drug−excipient interaction. The DSC curves of the pure drug, CHS, sodium ALG, and formulation are shown in Figure 4A−D. The pure BER exhibited the sharp endothermic peak at melting points of 139, 199.5, and 217.14 °C expressing the crystalline state of BER in pure drug (Figure 4A).[55] The endothermic curve for CHS disclosed at a melting point of 101.96 °C (Figure 4B). The DSC endothermic curve of sodium ALG appeared close to the curve of chitosan at 100 °C (Figure 4C) due to dehydration, followed by decomposition of the biopolymer at a melting point of 191.23 °C and above, respectively.[56] Moreover, the complex formation between sodium ALG and CHS causing entrapment of BER and thus the thermogram of DSC for the drug disappeared in the formulation, evidently expressing the converting crystalline structure in amorphous state of drug (Figure 4D).[57] The melting point of ALG in the formulation was slightly lowered and appeared at 75 °C and that of CHS obtained at 100 °C.

3.2.3. FTIR Spectral Analysis. The interaction among the excipients used in the formulation alongside the drug was physicochemically assessed using the FTIR spectrum for the chemical stability of the drug. The spectra of an individual compound such as drug, sodium ALG, CHS, and BER−ALG/CHS-NPs are expressed in Figure 5A−D. BER exhibited a specific absorption band at 3059 cm^{-1} due to C−H stretching, 2935.66 cm^{-1} due to C−H stretching, 2850.79 cm^{-1} due to −C−H stretching, 2123.63 cm^{-1} due to weak C≡C stretching, 1940.39 cm^{-1} due to weak C−H stretching, 1799.59 cm^{-1} due to C═O stretching, 1618.28 cm^{-1} due to strong C═C stretching, 1492.90 cm^{-1} stretching due to the aromatic C═C ring, 1388.75 cm^{-1} due to C═C stretching, peak at 1122.59−1037.70 cm^{-1} due to strong C−O stretching, and 910.47 cm^{-1} due to C═C bending vibration.

The absorption peak appeared at 14175.68 cm^{-1} (OH bending), 1298.09, and 1028.06 cm^{-1} (C−O stretching) from the surface-coated CHS molecules. The majority of drug peaks disappeared or showed reduced intensity in formulation BER−ALG/CHS-NPs, indicating reduced crystallinity of the drug following complexation with CHS/ALG. Therefore, the IR spectrum of BER−ALG/CHS-NPs affirmed DSC results. Further, the developed formulation substantially presented the chemical stability of the drug within the CHS/ALG complex. The spectral analysis noticed was comparative with the formerly reported studies in the BER-carried gelatin/sodium ALG complex.[58]

3.2.4. X-ray Diffraction Study. To investigate the crystal structure of the drug in the pure state and conversion into the molecular state in the formulation and compare with the pure drug, X-ray analysis was executed as shown in Figure 6A,B. The sharp and intense diffraction peak of pure BER was observed at 2θ of 8.71, 9.21, 16.40, 24.76, 25.6068, and 26.36°, suggesting the crystalline physical state of the drug (Figure 5A). On the other hand, the characteristic X-rays diffraction peak also observed in the formulation with reduced intensity at 2θ angles of 18.85, 19.28, 20.32, 21.23, 23.36, 23.56, and 29.36° (Figure 5B), corroborating that the crystalline nature of the drug substance may be converted into the amorphous or molecular state inside the polymeric core of the NPs.[59,60]

3.3. Dissolution Studies. The cumulative quantity of the drug liberated from the drug suspension and the formulation BER−ALG/CHS-NPs at a predetermined time separation is

https://doi.org/10.1021/acsomega.3c01153
ACS Omega 2023, 8, 38806−38821

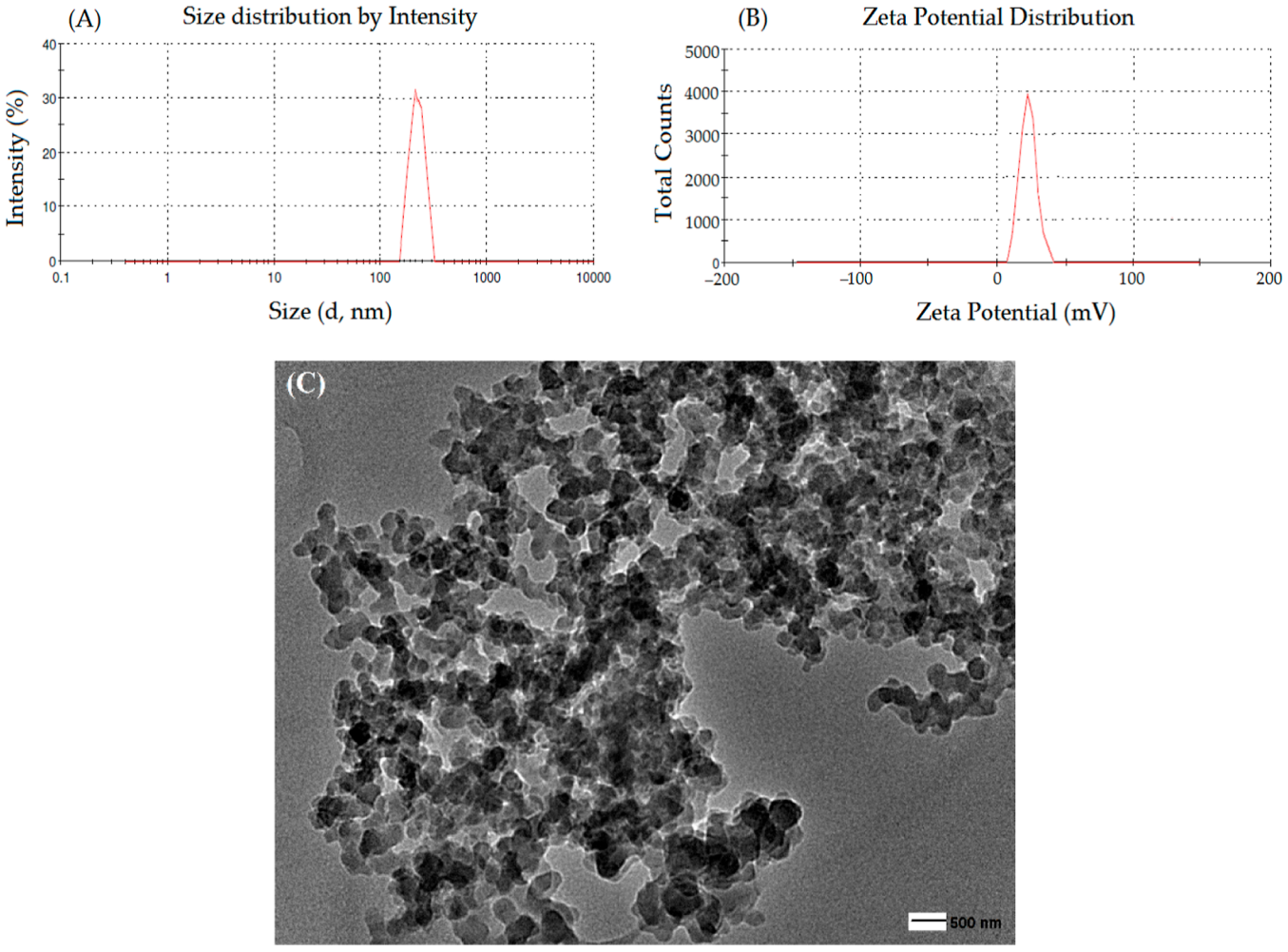

Figure 3. Particle size distribution histogram of (A), zeta potential curve of BER−ALG/CHS-NPs−F (B), and TEM image of BER−ALG/CHS-NPs−F (C).

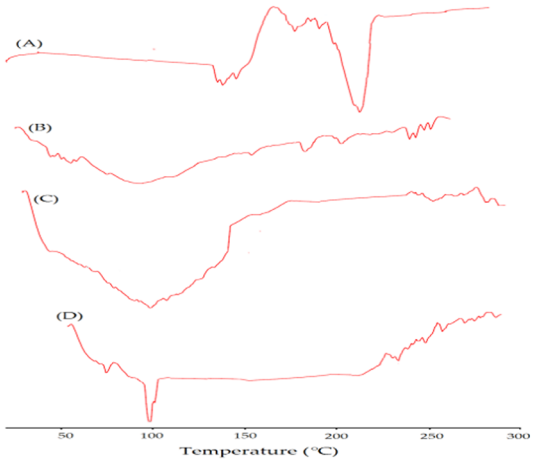

Figure 4. DSC curve of BER (A); sodium ALG (B); CHS (C); and BER−ALG/CHS-NPs−F(D) expressing the melting point of the compound.

expressed in Figure 7A,B. The drug release was commencing at zero time point, and the endpoint was obtained after completing 24 h. During this period, the release profile was assessed individually from BER−suspension and formulation. The initial burst release from the formulation was noticed for a period of 2 h up to 27 ± 3% in pH 7.4 (PBS) and 43 ± 7% in pH 5.5 (mimicking endosomal pH of the tumor) due to solubilization of the weakly held drug from the polymeric surface. Afterward, experienced drug liberation in a sustained manner for a period of 24 h in either of the media, i.e., 69.6 ± 12.3%, in physiological pH 7.4 and 87.9 ± 7% release took place at pH 5.5. Contrarily, the BER−suspension liberated approximately of 35 ± 7% drug content rapidly within 8 h and thereafter 48.8 ± 13% drug released in 24 h at pH 7.4 and similarly 56 ± 11% drug liberated in pH 5.5 at the end of 24 h. The rapid drug release from the BER−suspension could be due to the unformulated physical state of BER and poor stability in biological circulation for long time as well. Surprisingly, drug release from BER−ALG/CHS-NPs−F at pH 5.5 simulating the endosomal pH of tumor had shown higher release than physiological pH 7.4. The higher drug liberated at pH 5.5 may be due to the enhanced drug−polymer complex breakdown in the acidic medium, followed by improved drug solubility and dissolution in the medium from the ALG polymeric core. Additionally, it is worthy to indicate here that the slightly acidic tumor environment helps in polymer swelling, thereby lowering the ionic interaction, which favors drug release. The drug liberation from the ALG/CHS nanoplatform here was in accord with many studies in the scientific domain.[61−63,71] The acidic pH also favors CHS swelling due to repulsive forces between calcium ion and CHS

https://doi.org/10.1021/acsomega.3c01153
ACS Omega 2023, 8, 38806−38821

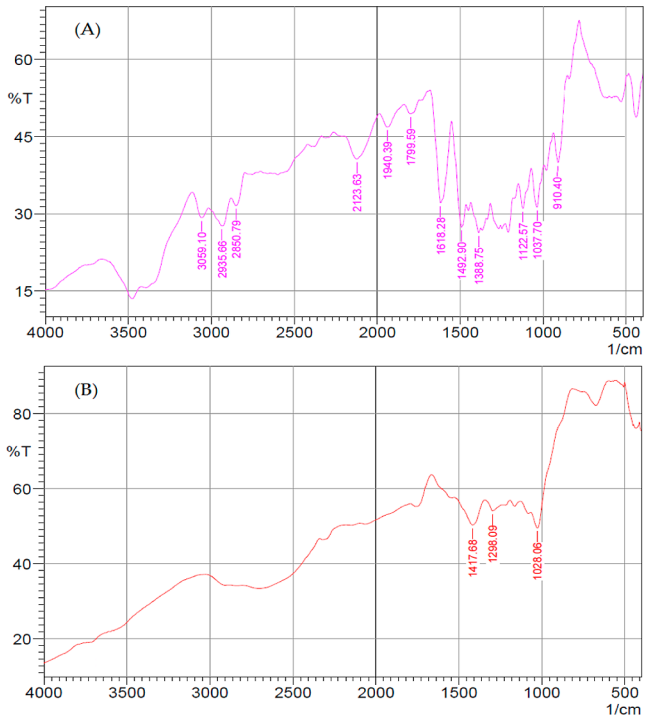

Figure 5. FTIR spectra of BER (A) and (B) BER−ALG/CHS-NPs−F (B).

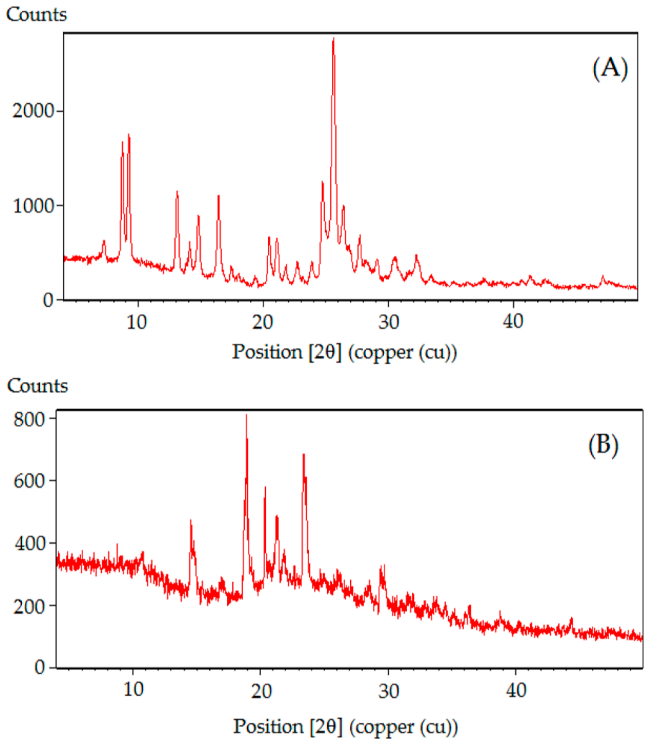

Figure 6. X-ray diffraction patterns of BER (A) and BER−ALG/CHS-NPs−F (B).

surface, which triggered improved solubilization of drug in pH 5.5 than physiological pH. The surface hydration of CHS in an aqueous medium result in swelling, and polymer complex erosion helps to increase drug liberation through the diffusion process. Moreover, drug liberation extended from the ALG/CHS core and also depends on the polymer concentration, pH, solubilization, and other physiological characteristics of the drug and nanocarrier system.[64]

The percentage drug liberated conformed to release the kinetic models to estimate the release mechanism from the nanocarrier system. The multiple release models were fitted to the release data such as the Higuchi model, zero order, first order, Korsmeyer−Peppas, and Hixson−Crowell and to ascertain the model with good fit (Table 6). The literature domain disclosed different types of kinetic model depicting the unlike drug release mechanism from the polymeric matrix.

The model was examined based on the regression value (R^2) from individual models. The best-fitted model was the Korsmeyer−Peppas model reported with highest coefficient of correlation (R^2 = 0.964). The swelling exponent (n) value calculated was 0.25 ($0.5 < n < 1$), relating to Fickian diffusion control of the drug release mechanism from the polymeric matrix. The controlled drug release from the polymeric carrier system was implicated by hydration, swelling, diffusion, and erosion of the dissolved drug from the polymeric matrix/core/layer. The drug release also facilitated by encompassing environment pH, dosing, physicochemical properties of the drug, and the nature of the polymer.[65,66]

3.4. Drug Permeation Analysis. The comparative studies of the surface-tailored formulation vs drug suspension outcomes are displayed in Figure 8. The intestinal permeation study revealed that the amount of drug permeated for the formulation was achieved significantly higher than the drug suspension. The highest amount of BER permeated from BER−ALG/CHS-NPs−F was determined as 82.5 ± 3.4 vs 19 ± 2.5 $\mu g/cm^2$ from the BER−suspension. The P_{app} of BER from the formulation across the membrane was 4.2 times higher than that of BER−suspension ($p < 0.01$). The positive charge surface of CHS due to the protonated amino group is desirable for the drug to be transported across the mucosa layer of the intestine, and this could be favored by the opposite charge on this layer, most probably through the biological interaction with the nanosurface area, leading to permeation through the tight junction of intestinal epithelia.[55,62]

3.5. In Vitro Cell Viability Assay. The cell toxicity investigation of the developed folate-ligated NPs and drug suspension was carried out by applying the MTT assay on the breast cancer cell line, MCF-7. This assay relied on the cellular reduction of the MTT dye (yellow color) to purple color. The reduction in cell viability following exposure of various concentrations of drug-encapsulated formulation and free drug was determined to be time and concentration dependent. Following 24 h of treatment with ligated formulation, the viable cells reduce to 42.2 ± 7%. On the other hand, the viable cells reduced to 79.6 ± 9% by drug suspension treatment during 24 h of incubation. Further, 48 h of incubation with different drug concentrations from the ligated formulation and drug suspension led to maximum inhibition of cells to 16.9 ± 6 and 73.9 ± 7.2%, respectively (Figure 9). It was further noted that the proliferation inhibition rate after 24 h from BER suspension was high, and by further increasing the incubation time to 48 h, progressive inhibition was not witnessed. Adversely, BER-loaded ligated formulation had shown tremendous improvement in inhibition of cell proliferation post-incubation with 48 h. MTT assay observation was comparable to the existing literature.[60,67,68] The IC_{50} values the of ligated formulation and drug suspension were determined from regression analysis of the % cell viability graph and estimated to be 34.8 ± 6 and 10.2 ± 2 μM and 22.7 ± 5 and 4.8 ± 1.2 μM at post-incubation

https://doi.org/10.1021/acsomega.3c01153
ACS Omega 2023, 8, 38806−38821

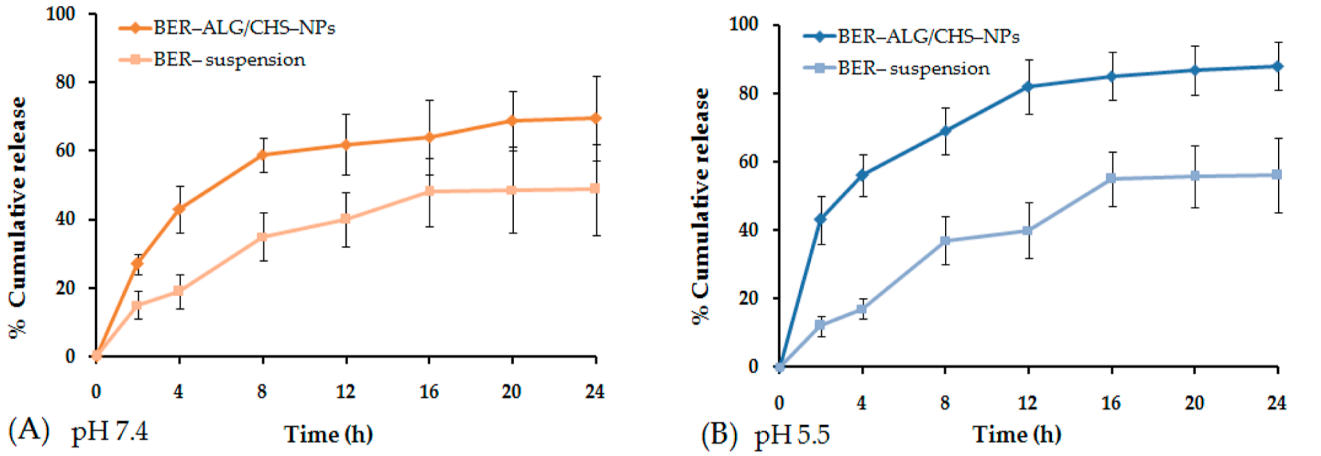

Figure 7. % Cumulative drug liberated from BER−suspension and BER−ALG/CHS-NPs−F (A) physiological pH 7.4 and (B) pH 5.5 simulating the tumor endosome.

Table 6. Kinetic Release Data for the Good Model Fit

Higuchi	Korsmeyer−Peppas	zero order	first order	Hixson Crowell	constants
0.76	0.964	0.800	0.696	0.753	R^2
0.34	0.25	0.67	0.56	0.78	n

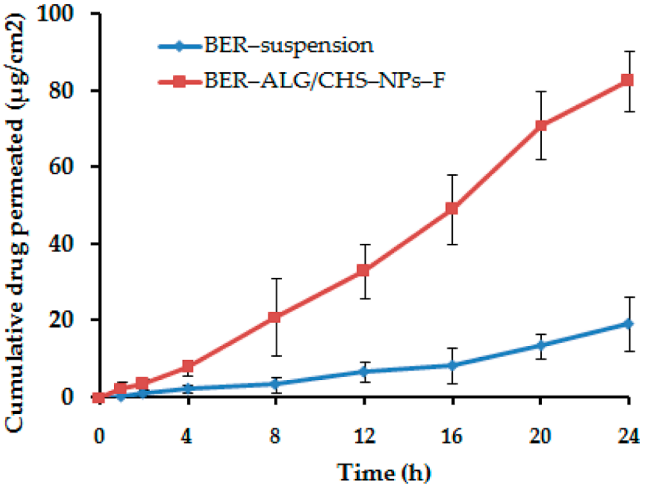

Figure 8. Drug permeation through the intestinal membrane of BER−suspension and BER−ALG/CHS-NPs−F. Data indicates mean ± SD experimented repeated three times (n = 3), (**$p \leq 0.05$) indicates significance level.

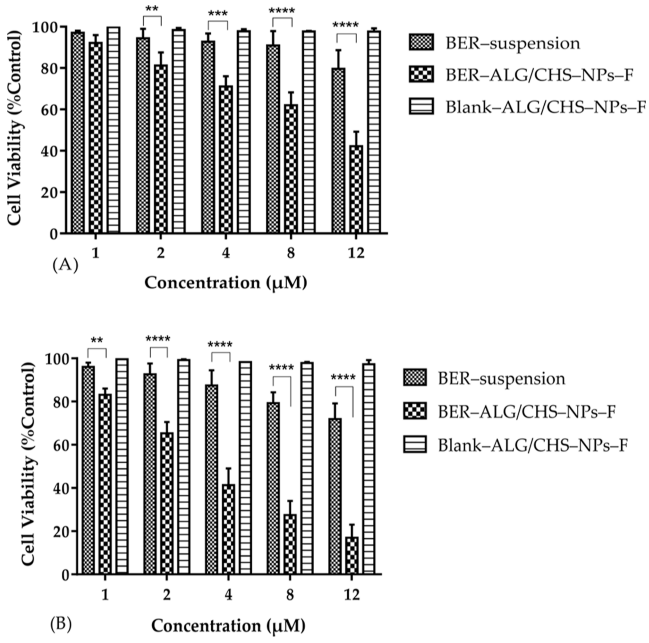

Figure 9. MTT assay post-incubation of ligated formulation and BER−suspension. The treatment drug dose was 1−12 μM to the MCF-7 cell line and incubated for 24 (A) and 48 h (B). Data shown as average ± SD in triplicate (n = 3). Results interpreted statistically using ANOVA and Tukey's analysis (**$p < 0.01$) and (****$p < 0.0001$) when BER−ALG/CHS-NPs−F are compared with BER−suspension.

times of 24 and 48 h, respectively (Figure 9A,B). Furthermore, the outcomes of cell viability assay pointed that the optimized ligated formulation was more toxic to the MCF-7 cell line relative to drug suspension ($p < 0.05$) of BER.

The nonengineered nanocarrier-based drug delivery aids with no specific recognition on their surface and have limited applicability, probably due to poor drug access and lack of satisfying targeting potential to the main domain. The drug access to the target region through high retention and drug permeation leads to the off-target effect and causes toxicity, resulting in harm to the normal cells.[8,69] To overcome them, specific targeting to the tumor microenvironment is desirable for payload release. The nanocarrier protects drug particles from degradation and provides biostability, thereby the drug content transported to the cells in the biological medium, and interacting with the protein components of blood fraction, and thus may show enhanced efficacy.[17] Adversely, surface-engineered NPs, BER−ALG/CHS-NPs−F, decorated with the ligand have specific recognition and bind actively with the overexpressed receptor located over the cell surface, ensuring the ligand−target interaction, thereby maximizing payload internalization and concomitantly reducing the warhead loss in the macrophagic system. The higher cytotoxic effect caused by the engineered NPs, BER−ALG/CHS-NPs−F, may be ascribed to the in-built inherent targeting potential of the nanocarrier, highly dissolving or molecular state of BER. Inversely, the BER−suspension showed poor cytotoxicity due to limited solubility and dissolution which circumscribed its metabolic activity.[6,16]

3.6. Cell Uptake Study. The breast cancer cell line was employed to determine the cellular uptake of BER from the formulation, BER−ALG/CHS-NPs−F, the and BER−suspen-

https://doi.org/10.1021/acsomega.3c01153
ACS Omega 2023, 8, 38806−38821

sion. The cellular uptake of BER−ALG/CHS-NPs−F and BER−suspension was determined to be 858.6 and 156.4 ng/μg, respectively [Figure 10]. The BER uptake from the formulation

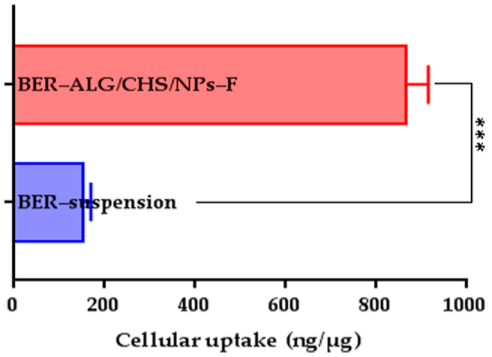

Figure 10. Comparative cellular uptake of BER−ALG/CHS-NPs−F and BER−suspension. Statistical comparison made by Student's *t*-test (two tailed) data shown, average ± SD (n = 3) significant level ***p < 0.0001.

was statistically different from that of the BER−suspension, and it was 5.5 times higher than that of the BER−suspension (p < 0.0001). The cell uptake of BER from the folate-ligated formulation was enormously high, which may be due to the folate grafting to the nanocarrier surface and leading to enhance uptake of therapeutics mediated through the folate receptor. It is a most important process at the cellular level having control over the biological activity of the molecules. The NP uptake mediated via a process of endocytosis. The uptake of the molecules largely relies on the process of the positive interaction between the carriers and the cell membrane. The process of cellular uptake is influenced by the physicochemical feature of NPs and varies from particle shape, size, charge, active moiety encapsulation, and stability of NPs in the biological system.[70]

3.7. In Vivo Evaluation. The preclinical investigation of optimized BER−ALG/CHS-NPs−F and BER−suspension was performed, and the pharmacokinetic parameters are determined. Figure 11 shows the BER mean plasma concentration−time profiles from BER−ALG/CHS-NPs−F and BBR−suspension after single-dose oral intake, and Table 7 indicates

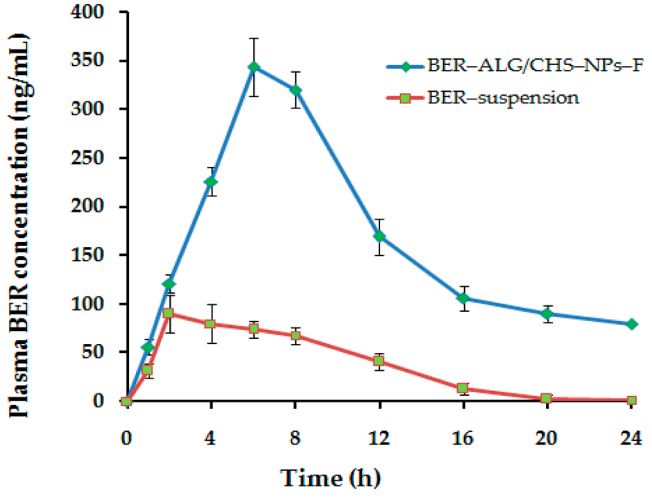

Figure 11. Plasma BER concentration from BER−ALG/CHS-NPs−F and BER−suspension on per oral administration.

Table 7. Investigated Pharmacokinetic Parameter of BER−ALG/CHS-NPs−F and BER−Suspension in Rat after Oral Intake of Single Dose of BER (n = 3, Mean ± S.D)

parameters	BER−ALG/CHS-NPs−F	BER−suspension
C_{max} (ng/mL)	344 ± 4.65	90 ± 2.7
T_{max} (h)	6 ± 0.1	2.00 ± 0.3
AUC_{0-t} (ng/mL*h)	3915 ± 15	890 ± 16.8
$t_{1/2}$ (h)	11 ± 0.03	3 ± 0.08
k_e (h^{-1})	0.34 ± 0.02	0.28 ± 0.04

various estimated pharmacokinetic parameters. Among the different parameter result of C_{max} showed 4-fold enhancement for BER−ALG/CHS-NPs−F compared to BER−suspension, i.e., 344 ± 4.65 ng/mL vs 90 ± 2.7 ng/mL concentration (p < 0.01). The maximum plasma concentration of BER from the suspension was achieved in a T_{max} of 2.00 ± 0.3, while delivering BER from the formulation achieved a maximum plasma concentration in a T_{max} of 6 ± 0.1. The higher T_{max} reported for the formulation may be attributed to the sustained release profile of BER (p < 0.01). The higher absorption from the optimized formulation is probably due to the better penetration and mucoadhesive nature of CHS and ALG and P-glycoprotein inhibition by ALG and CHS polymers in the formulation. The extent of drug absorption indicated as areas under the curve (AUC_{0-24}), i.e., bioavailability of BER−suspension and BER−ALG/CHS-NPs−F, was determined to be 3915 ± 15 and 890 ± 16.8 ng/mL*h for BER−ALG/CHS-NPs−F and BER−suspension, respectively. It indicates a significant absorption of BER from the nanocarrier than unformulated BER (p < 0.05). The improvement in the oral bioavailability of the BER from the optimized formulation revealed 4.4-fold higher vis-à-vis to BER−suspension. The pharmacokinetic parameter evaluation can be compared to the oral BER−phospholipid complex and bioavailability enhancement of BER.[62,71,72] Therefore, the developed formulation could help to absorb BER from BER−ALG/CHS-NPs−F and may be exploited for therapeutic application of BER. The $t_{1/2}$ of the BER−suspension was found to be 3 ± 0.08 h, which increased to 11 ± 0.03 h in BER−ALG/CHS-NPs−F. The elimination rate, k_e (h^{-1}), of BER−ALG/CHS-NPs−F and BER−suspension was estimated to be 0.34 ± 0.02 and 0.28 ± 0.04 h^{-1}, respectively.

3.8. Hemolysis Assay. The biocompatibility of the fabricated formulation BER−ALG/CHS-NPs−F was investigated to ascertain the hemocompatibility of the produced NPs in systemic circulation and to elicit the % hemolysis due to red blood cell (RBC) destruction. The destruction in RBC is due to the cytotoxic nature of the nanomaterials in the biological system. The NPs in contact with blood circulation interact with various cell components foremost with RBC and causing damage and thus released hemoglobin. The hemolytic study observed that destruction of RBC was less than 2% and consider the safe administration of the produced NPs. As per the ASTMF756-00 (2000) standard, the materials considered to be nonhemolytic, when the percentage hemolysis is less than 2%. This could be attributed to the natural sources of the biomaterial used in the study.[73]

3.9. DPPH Radical Scavenging Assay. The measurement of the antioxidant capacity of photoactive and biological compounds using the DPPH assay is widely employed in radical scavenging activity measurement.[74] DPPH is a proton acceptor (H^+) from the sample compound and acts as a free radical. The free radical from the DPPH assay makes the dark purple color of

https://doi.org/10.1021/acsomega.3c01153
ACS Omega 2023, 8, 38806−38821

solution and treatment with the compound having an antioxidant property, making them colorless. It is apparently said from the results incurred that BER in their pure state is not a good antioxidant, although the radical quenching capacity of it was enhanced in the nanoformulation. This may be due to improved solubility and dissolution of the hydrophobic drug encapsulated in the nanocomposite. The antioxidant capacities of the BER−ALG/CHS-NPs−F vs BER−suspension were measured to be 62.3 ± 2.5% vs 30 ± 6%. The blank ALG/CHS-NPs−F and positive control Asc (ascorbic) were reported to be 17.67 ± 3.7 and 98.89% (Figure 12). The antioxidant

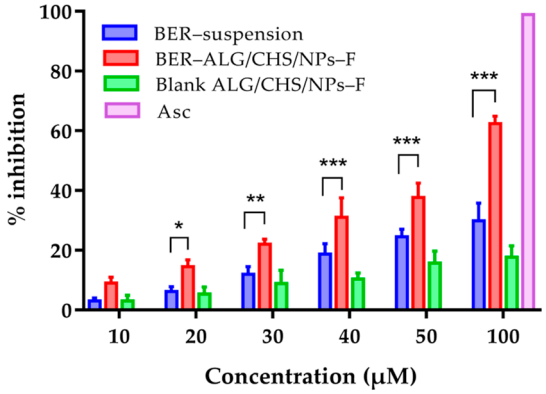

Figure 12. Antioxidant activity by the DPPH assay showing % inhibition by BER−ALG/CHS-NPs−F, BER−suspension, positive control: Asc, blank ALG/CHS-NPs−F. Experiment repeated thrice (n = 3) ±SD. *p < 0.05; **p < 0.01; and ***p < 0.001, when BER−ALG/CHS-NPs−F compared with BER−suspension. (Significant statistical differences considered when, p < 0.05).

capacity of the nanocomposite was significantly higher than the drug suspension (p < 0.05). The antioxidant capacity of BER in their suspension and formulation was determined to be concentration dependent; however, higher antioxidant activity accounted for the nanocomposite, which may be due to the dissolved drug in the polymeric matrix which protects against a harsh biological environment and maintains the stability. In fact, the antioxidant power of pure BER was not progressively increased with increasing their concentration after 50 μM, which may be due to the unformulated or poorly dissolved state of it. The radial quenching capacity of BER is found out, which is comparable to the formerly cited literature.[44,75]

3.10. Stability of Formulation. The experimental observation of the colloidal stability of BER−ALG/CHS/NPs−F is expressed in Figure 13. The stability of the optimized formulation evaluated for the given period and changes in the formulation characteristics related to particles size (nm), PDI, and drug entrapment in the formulation were noted. The particle size in the nanosystem kept on growing as the increase in the number of days during storage may be due to the chances of particle agglomeration, but the extent of particle size growth was not significant (p > 0.05). Further, the PDI of formulation was slightly increased due to particle agglomeration; although, the monodispersity index of the formulation remains unaltered. The alteration in the physical properties was statistically not significant, stating that the formulation generated remains stable for the said time (p > 0.05). The drug entrapment was noticed to decrease on increasing storage time. The hydration of the particle in the aqueous medium may lead to chances of drug leak

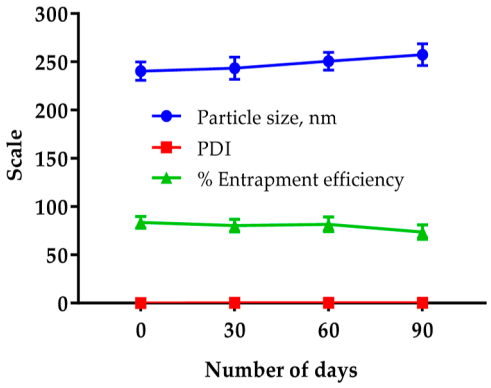

Figure 13. Stability measurement of ligated formulation with respect to physical changes in particle size, PDI, and % EE for the assigned time at room temperature (25 ± 2 °C).

out from the polymeric matrix, which could be a reason for decrement in drug entrapment.[15]

4. CONCLUSIONS

The developed ligated formulation of BER was characterized and investigated in vitro for the chosen parameters, which showed improved drug release, stability, as well as enhanced % inhibition in the MCF-7 cell line in comparison to drug suspension. The in-house developed ligated formulation was optimized, implementing the design of the experiment, which apparently explained the impact of input attributes such as concentration of CHS (X1), sodium ALG (X2), and sonication time (X3) at the designated level onto the important parameters of formulation or responses such as particle size (Y1) and % EE (Y3). The optimum concentration of the developed formulation was robust and stable having a composition of (CHS, X1 = 10 mg; sodium ALG, X2 = 27.8 mg; and sonication time, X3 = 9.15 min). The narrow particle size distribution determined by the Zetasizer expressed homogeneity and consistent preparation and further confirmed by the TEM study, which revealed uniform shape and size and well dispersed in the preparation. The polymeric matrix controlled the drug release in the conterminous environment through the diffusion process and showed improved release in pHs 7.4 and pH 5.5 for the intended time. The Korsmeyer−Peppas was the best fitted kinetic model following Fickian diffusion, which was revealed based on the regression coefficient value (R^2 = 0.964). Furthermore, thermal and spectral analysis showed that formulating excipient drug was compatible and stable in the formulation. The intestinal permeation study reported high permeation rate of BER from the designed nanocarrier than free the drug. The MTT assay brought out significant cell toxicity caused by the developed ligated formulation than the free drug. To the end, the ligated formulation was stable for the aforesaid period under normal temperature. The findings interpreted that the produced ligated nanocarrier bearing BER could be an option in the management of breast cancer therapy.

AUTHOR INFORMATION

Corresponding Author

Obaid Afzal − *Department of Pharmaceutical Chemistry, College of Pharmacy, Prince Sattam Bin Abdulaziz University, Al-Kharj 11942, Saudi Arabia;* orcid.org/0000-0002-4188-5592; Email: o.akram@psau.edu.sa, obaid263@gmail.com

https://doi.org/10.1021/acsomega.3c01153
ACS Omega 2023, 8, 38806−38821

Authors

Mushtaq Ahmad Mir − *Department of Clinical Laboratory Sciences, College of Applied Medical Sciences, King Khalid University, Abha 62521, Saudi Arabia*

Md Habban Akhter − *School of Pharmaceutical and Population Health Informatics (SoPPHI), DIT University, Dehradun 248009, India*

Safia Obaidur Rab − *Department of Clinical Laboratory Sciences, College of Applied Medical Sciences, King Khalid University, Abha 62521, Saudi Arabia*

Abdulmalik S. A. Altamimi − *Department of Pharmaceutical Chemistry, College of Pharmacy, Prince Sattam Bin Abdulaziz University, Al-Kharj 11942, Saudi Arabia*

Manal A. Alossaimi − *Department of Pharmaceutical Chemistry, College of Pharmacy, Prince Sattam Bin Abdulaziz University, Al-Kharj 11942, Saudi Arabia*

Shehla Nasar Mir Najib Ullah − *Department of Pharmacognosy, Faculty of Pharmacy, King Khalid University, Abha 62521, Saudi Arabia*

Mariusz Jaremko − *Smart-Health Initiative (SHI) and Red Sea Research Center (RSRC), Division of Biological and Environmental Sciences and Engineering (BESE), King Abdullah University of Science and Technology (KAUST), Thuwal 23955, Saudi Arabia*

Abdul-Hamid Emwas − *Core Labs, King Abdullah University of Science and Technology (KAUST), Thuwal 23955, Saudi Arabia*

Sarfaraz Ahmad − *Department of Clinical Pharmacy, College of Pharmacy, Jazan University, Jazan 45142, Saudi Arabia*

Nawazish Alam − *Department of Clinical Pharmacy, College of Pharmacy, Jazan University, Jazan 45142, Saudi Arabia*

Md Sajid Ali − *Department of Pharmaceutics, College of Pharmacy, Jazan University, Jazan 45142, Saudi Arabia*

Complete contact information is available at: https://pubs.acs.org/10.1021/acsomega.3c01153

Author Contributions

M.H.A., M.A.M., and O.A. contributed to conceptualization; M.H.A., O.A., S.O.R., and M.A.M. contributed to data curation; S.O.R., A.S.A.A., M.A.A., M.J., A.H.E., S.A., and N.A. contributed to formal analysis; S.O.R. and A.H.E. contributed to funding acquisition; M.A.M., M.H.A., O.A., N.A., and M.S.A. contributed to investigation; M.A.M., A.S.A.A., M.H.A., M.A.A., S.N.M.N.U., and M.S.A. contributed to methodology; M.H.A., S.O.R., and N.A. contributed to project administration; M.J., A.S.A.A., and A.H.E. contributed to resources; M.H.A. and S.A. contributed to software; O.A., N.A., and A.H.E. contributed to supervision; O.A., S.N.M.N.U., and M.S.A. contributed to validation; M.A.M., M.J., A.-H.E., S.A., and A.S.A.A. contributed to visualization; M.H.A., O.A., and M.A.M. contributed to writing—original draft; and M.H.A., M.J., M.A.A., A.S.A.A., and A.H.E. contributed to writing—review & editing. All authors have read and agreed to the published version of the manuscript.

Notes

The authors declare no competing financial interest.

■ ACKNOWLEDGMENTS

The authors express their gratitude to the Deanship of Scientific Research at King Khalid University for funding this work through the Large Research Group Project under grant number RGP.02/339/44.

■ REFERENCES

(1) Siegel, R. L.; Miller, K. D.; Fuchs, H. E.; Jemal, A. Cancer statistics, 2022. *Ca-Cancer J. Clin.* **2022**, *72*, 7−33.

(2) Akhter, M. H.; Madhav, N. S.; Ahmad, J. Epidermal growth factor based active targeting: A paradigm shift towards advance tumor therapy. *Artif. Cells, Nanomed., Biotechnol.* **2018**, *46*, 1188−1198.

(3) Ji, X.; Lu, Y.; Tian, H.; Meng, X.; Wei, M.; Cho, W. C. Chemoresistance mechanisms of breast cancer and their countermeasures. *Biomed. Pharm.* **2019**, *114*, 108800.

(4) Bae, Y. H. Drug targeting and tumor heterogeneity. *J. Controlled Release* **2009**, *133*, 2−3.

(5) Rizvi, S. A. A.; Saleh, A. M. Applications of nanoparticle systems in drug delivery technology. *Saudi Pharm. J.* **2018**, *26*, 64−70.

(6) Ahmad, J.; Ameeduzzafar; Ahmad, M. Z.; Akhter, H. Surface-Engineered Cancer Nanomedicine: Rational Design and Recent Progress. *Curr. Pharm. Des.* **2020**, *26*, 1181−1190.

(7) Afrooz, H.; Ahmadi, F.; Fallahzadeh, F.; Mousavi-Fard, S. H.; Alipour, S. Design and characterization of paclitaxel-verapamil co-encapsulated PLGA nanoparticles: Potential system for overcoming P-glycoprotein mediated MDR. *J. Drug Delivery Sci. Technol.* **2017**, *41*, 174−181.

(8) Akhter, M. H.; Rizwanullah, M.; Ahmad, J.; Ahsan, M. J.; Mujtaba, A.; Amin, S. Nano carriers in advanced drug targeting: Setting novel paradigm in cancer therapeutics. *Artif. Cells, Nanomed., Biotechnol.* **2018**, *46*, 873−884.

(9) Teixeira, S.; Carvalho, M. A.; Castanheira, E. M. S. Functionalized Liposome and Albumin-Based Systems as Carriers for Poorly Water-Soluble Anticancer Drugs: An Updated Review. *Biomedicines* **2022**, *10*, 486.

(10) Cui, Y.; Xu, Q.; Chow, P. K.; Wang, D.; Wang, C. H. Transferrin-conjugated magnetic silica PLGA nanoparticles loaded with doxorubicin and paclitaxel for brain glioma treatment. *Biomaterials* **2013**, *34*, 8511−8520.

(11) Iqbal, H.; Razzaq, A.; Khan, N. U.; Rehman, S. U.; Webster, T. J.; Xiao, R.; Menaa, F. pH-responsive albumin-coated biopolymeric nanoparticles with lapatinab for targeted breast cancer therapy. *Biomater. Adv.* **2022**, *139*, 213039.

(12) Zhang, M.; Zhu, J.; Zheng, Y.; Guo, R.; Wang, S.; Mignani, S.; Caminade, A. M.; Majoral, J. P.; Shi, X. Doxorubicin-Conjugated PAMAM Dendrimers for pH-Responsive Drug Release and Folic Acid-Targeted Cancer Therapy. *Pharmaceutics* **2018**, *10*, 162.

(13) Hailing, Y.; Xiufang, L.; Lili, W.; Baoqiang, L.; Kaichen, H.; Yongquan, H.; Qianqian, Z.; Chaoming, M.; Xiaoshuai, R.; Rui, Z.; Hui, L.; Pengfei, P.; Hong, S. Doxorubicin-loaded fluorescent carbon dots with PEI passivation as a drug delivery system for cancer therapy. *Nanoscale* **2020**, *12*, 17222−17237.

(14) Awan, U. A.; Raza, A.; Ali, S.; Saeed, R. F.; Akhtar, N. Doxorubicin-loaded gold nanorods: a multifunctional chemo-photothermal nanoplatform for cancer management. *Beilstein J. Nanotechnol.* **2021**, *12*, 295−303.

(15) Afzal, O.; Akhter, M. H.; Ahmad, I.; Muzammil, K.; Dawria, A.; Zeyaullah, M.; Altamimi, A. S. A.; Khalilullah, H.; Mir Najib Ullah, S. N.; Rahman, M. A.; Ali, A.; Shahzad, N.; Jaremko, M.; Emwas, A.-H.; Abdel Aziz Ibrahim, I. A *β*−Sitosterol Encapsulated Biocompatible Alginate/Chitosan Polymer Nanocomposite for the Treatment of Breast Cancer. *Pharmaceutics* **2022**, *14*, 1711.

(16) Akhter, M. H.; Beg, S.; Tarique, M.; Malik, A.; Afaq, S.; Choudhry, H.; Hosawi, S. Receptor-based targeting of engineered nanocarrier against solid tumors: Recent progress and challenges ahead. *Biochim. Biophys. Acta, Gen. Subj.* **2021**, *1865*, 129777.

(17) Akhter, M. H.; Khalilullah, H.; Gupta, M.; Alfaleh, M. A.; Alhakamy, N. A.; Riadi, Y.; Md, S. Impact of Protein Corona on the Biological Identity of Nanomedicine: Understanding the Fate of Nanomaterials in the Biological Milieu. *Biomedicines* **2021**, *9*, 1496.

(18) Poulson, B. G.; Alsulami, Q. A.; Sharfalddin, A.; El-Agammy, E. F.; Mouffouk, F.; Emwas, A.-H.; Jaremko, L.; Jaremko, M. Cyclodextrins: Structural, Chemical, and Physical Properties, and Applications. *Polysaccharides* **2021**, *3*, 1−31.

(19) Dhahri, M.; Alghrably, M.; Mohammed, H. A.; Badshah, S. L.; Noreen, N.; Mouffouk, F.; Rayyan, S.; Qureshi, K. A.; Mahmood, D.; Lachowicz, J. I.; Jaremko, M.; Emwas, A.-H. Natural Polysaccharides as Preventive and Therapeutic Horizon for Neurodegenerative Diseases. *Pharmaceutics* **2021**, *14*, 1.
(20) Dhahri, M.; Sioud, S.; Dridi, R.; Hassine, M.; Boughattas, N. A.; Almulhim, F.; Al Talla, Z.; Jaremko, M.; Emwas, A.-H. Extraction, Characterization, and Anticoagulant Activity of a Sulfated Polysaccharide from Bursatellaleachii Viscera. *ACS Omega* **2020**, *5*, 14786−14795.
(21) Mohammed, M. A.; Syeda, J. T. M.; Wasan, K. M.; Wasan, E. K. An Overview of Chitosan Nanoparticles and Its Application in Non-Parenteral Drug Delivery. *Pharmaceutics* **2017**, *9*, 53.
(22) Herdiana, Y.; Wathoni, N.; Shamsuddin, S.; Joni, I. M.; Muchtaridi, M. Chitosan-Based Nanoparticles of Targeted Drug Delivery System in Breast Cancer Treatment. *Polymers* **2021**, *13*, 1717.
(23) Borgogna, M.; Skjåk-Bræk, G.; Paoletti, S.; Donati, I. On the initial binding of alginate by calcium ions. The tilted egg-box hypothesis. *J. Phys. Chem. B* **2013**, *117*, 7277−7282.
(24) Niang, P. M.; Huang, Z.; Dulong, V.; Souguir, Z.; Le Cerf, D.; Picton, L. Thermo-controlled rheology of electro-assembled polyanionic polysaccharide (alginate) and polycationic thermo-sensitive polymers. *Carbohydr. Polym.* **2016**, *139*, 67−74.
(25) Pedroso-Santana, S.; Fleitas-Salazar, N. Ionotropic gelation method in the synthesis of nanoparticles/microparticles for biomedical purposes. *Polym. Int.* **2020**, *69*, 443−447.
(26) Sun, Y.; Wang, W.; Tong, Y. Berberine Inhibits Proliferative Ability of Breast Cancer Cells by Reducing Metadherin. *Med. Sci. Monit.* **2019**, *25*, 9058−9066.
(27) Kausar, H.; Mujeeb, M.; Ahad, A.; Moolakkadath, T.; Aqil, M.; Ahmad, A.; Akhter, M. H. Optimization of ethosomes for topical thymoquinone delivery for the treatment of skin acne. *J. Drug Delivery Sci. Technol.* **2019**, *49*, 177−187.
(28) Md, S.; Alhakamy, N. A.; Aldawsari, H. M.; Husain, M.; Khan, N.; Alfaleh, M. A.; Asfour, H. Z.; Riadi, Y.; Bilgrami, A. L.; Akhter, M. H. Plumbagin-Loaded Glycerosome Gel as Topical Delivery System for Skin Cancer Therapy. *Polymers* **2021**, *13*, 923.
(29) Karim, S.; Akhter, M. H.; Burzangi, A. S.; Alkreathy, H.; Alharthy, B.; Kotta, S.; Md, S.; Rashid, M. A.; Afzal, O.; Altamimi, A. S. A.; Khalilullah, H. Phytosterol-Loaded Surface-Tailored Bioactive-Polymer Nanoparticles for Cancer Treatment: Optimization, In Vitro Cell Viability, Antioxidant Activity, and Stability Studies. *Gels* **2022**, *8*, 219.
(30) Md, S.; Alhakamy, N. A.; Neamatallah, T.; Alshehri, S.; Mujtaba, M. A.; Riadi, Y.; Radhakrishnan, A. K.; Khalilullah, H.; Gupta, M.; Akhter, M. H. Development, Characterization, and Evaluation of α-Mangostin-Loaded Polymeric Nanoparticle Gel for Topical Therapy in Skin Cancer. *Gels* **2021**, *7*, 230.
(31) Akhter, M. H.; Kumar, S.; Nomani, S. Sonication tailored enhance cytotoxicity of naringenin nanoparticle in pancreatic cancer: Design, optimization, and in vitro studies. *Drug Dev. Ind. Pharm.* **2020**, *46*, 659−672.
(32) Soni, K.; Mujtaba, A.; Akhter, M. H.; Zafar, A.; Kohli, K. Optimisation of ethosomal nanogel for topical nano-CUR and sulphoraphane delivery in effective skin cancer therapy. *J. Microencapsulation* **2019**, *37*, 91−108.
(33) Wang, Y.; Liu, Y.; Du, X.; Ma, H.; Yao, J. Berberine reverses doxorubicin resistance by inhibiting autophagy through the PTEN/Akt/mTOR signaling pathway in breast Cancer. *OncoTargets Ther.* **2020**, *13*, 1909−1919.
(34) Wang, Y.; Liu, Y.; Du, X.; Ma, H.; Yao, J. The Anti-Cancer Mechanisms of Berberine: A Review. *Cancer Manage. Res.* **2020**, *12*, 695−702.
(35) Gao, X.; Wang, J.; Li, M.; Wang, J.; Lv, J.; Zhang, L.; Sun, C.; Ji, J.; Yang, W.; Zhao, Z.; Mao, W. Berberine attenuates XRCC1-mediated base excision repair and sensitizes breast cancer cells to the chemotherapeutic drugs. *J. Cell. Mol. Med.* **2019**, *23*, 6797−6804.
(36) Ahmadiankia, N.; Moghaddam, H. K.; Mishan, M. A.; Bahrami, A. R.; Naderi-Meshkin, H.; Bidkhori, H. R.; Moghaddam, M.; Mirfeyzi, S. J. A. Berberine suppresses migration of MCF-7 breast cancer cells through down-regulation of chemokine receptors. *Iran. J. Basic Med. Sci.* **2016**, *19*, 125.
(37) Yu, H. H.; Kim, K. J.; Cha, J. D.; Kim, H. K.; Lee, Y. E.; Choi, N. Y.; You, Y. O. Antimicrobial activity of berberine alone and in combination with ampicillin or oxacillin against methicillin-resistant Staphylococcus aureus. *J. Med. Food* **2005**, *8*, 454−461.
(38) Wei, X.; Wang, C.; Hao, S.; Song, H.; Yang, L. The therapeutic effect of berberine in the treatment of nonalcoholic fatty liver disease: A meta-analysis. *J. Evidence-Based Complementary Altern. Med.* **2016**, *2016*, 3592951−3592959.
(39) Zhang, Y.; Li, X.; Zou, D.; Liu, W.; Yang, J.; Zhu, N.; Huo, L.; Wang, M.; Hong, J.; Wu, P.; Ren, G.; Ning, G. Treatment of type 2 diabetes and dyslipidemia with the natural plant alkaloid berberine. *J. Clin. Endocrinol. Metab.* **2008**, *93*, 2559−2565.
(40) Xie, J.; Xu, Y.; Huang, X.; Chen, Y.; Fu, J.; Xi, M.; Wang, L. Berberine-induced apoptosis in human breast cancer cells is mediated by reactive oxygen species generation and mitochondrial-related apoptotic pathway. *Tumor Biol.* **2015**, *36*, 1279−1288.
(41) Ansari, M. J.; Rahman, M.; Alharbi, K. S.; Altowayan, W. M.; Ali, A. M. A.; Almalki, W. H.; Barkat, M. A.; Singh, T.; Nasar, S.; Akhter, M. H.; Beg, S.; Choudhry, H. Hispolon-Loaded Liquid Crystalline Nanoparticles: Development, Stability, In Vitro Delivery Profile, and Assessment of Hepatoprotective Activity in Hepatocellular Carcinoma. *ACS Omega* **2022**, *7*, 9452−9464.
(42) Hernández-Ramírez, J. O.; Nava-Ramírez, M. J.; Merino-Guzmán, R.; Téllez-Isaías, G.; Vázquez-Durán, A.; Méndez-Albores, A. The effect of moderate-dose aflatoxin B 1 and Salmonella Enteritidis infection on intestinal permeability in broiler chickens. *Mycotoxin Res.* **2020**, *36*, 31−39.
(43) Gilani, S.; Chrystal, P. V.; Barekatain, R. Current experimental models, assessment and dietary modulations of intestinal permeability in broiler chickens. *Anim. Nutr.* **2021**, *7*, 801−811.
(44) Rajasekhar, K.; Samanta, S.; Bagoband, V.; Murugan, N. A.; Govindaraju, T. Antioxidant Berberine-Derivative Inhibits Multifaceted Amyloid Toxicity. *iScience* **2020**, *23*, 101005.
(45) Akhter, M. H.; Ahmad, A.; Ali, J.; Mohan, G. Formulation and Development of CoQ10-Loaded s-SNEDDS for Enhancement of Oral Bioavailability. *J. Pharm. Innovation* **2014**, *9*, 121−131.
(46) Aman, R. M.; Abu Hashim, I. I.; Meshali, M. M. Novel chitosan-based solid-lipid nanoparticles to enhance the bio-residence of the miraculous phytochemical "Apocynin". *Eur. J. Pharm. Sci.* **2018**, *124*, 304−318.
(47) Caetano, L. A.; Almeida, A. J.; Gonçalves, L. M. Effect of Experimental Parameters on Alginate/Chitosan Microparticles for BCG Encapsulation. *Mar. Drugs* **2016**, *14*, 90.
(48) Loquercio, A.; Castell-Perez, E.; Gomes, C.; Moreira, R. G. Preparation of Chitosan-Alginate Nanoparticles for Trans-cinnamaldehyde Entrapment. *J. Food Sci.* **2015**, *80*, N2305−N2315.
(49) Lang, X.; Wang, T.; Sun, M.; Chen, X.; Liu, Y. Advances and applications of chitosan-based nanomaterials as oral delivery carriers: A review. *Int. J. Biol. Macromol.* **2020**, *154*, 433−445.
(50) Song, W.; Su, X.; Gregory, D. A.; Li, W.; Cai, Z.; Zhao, X. Magnetic Alginate/Chitosan Nanoparticles for Targeted Delivery of Curcumin into Human Breast Cancer Cells. *Nanomaterials* **2018**, *8*, 907.
(51) Alfatama, M.; Lim, L. Y.; Wong, T. W. Alginate-C18 conjugate nanoparticles loaded in tripolyphosphate-cross-linked chitosan-oleic acid conjugate-coated calcium alginate beads as oral insulin carrier. *Mol. Pharm.* **2018**, *15*, 3369−3382.
(52) Afzali, E.; Eslaminejad, T.; Yazdi Rouholamini, S. E.; Shahrokhi-Farjah, M.; Ansari, M. Cytotoxicity Effects of Curcumin Loaded on Chitosan Alginate Nanospheres on the KMBC-10 Spheroids Cell Line. *Int. J. Nanomed.* **2021**, *16*, 579−589.
(53) Azevedo, M. A.; Bourbon, A. I.; Vicente, A. A.; Cerqueira, M. A. Alginate/chitosan nanoparticles for encapsulation and controlled release of vitamin B2. *Int. J. Biol. Macromol.* **2014**, *71*, 141−146.
(54) Mahya, S.; Ai, J.; Shojae, S.; Khonakdar, H. A.; Darbemamieh, G.; Shirian, S. Berberine loaded chitosan nanoparticles encapsulated in

https://doi.org/10.1021/acsomega.3c01153
ACS Omega 2023, 8, 38806−38821

polysaccharide-based hydrogel for the repair of spinal cord. *Int. J. Biol. Macromol.* **2021**, *182*, 82−90.
(55) Niu, J.; Yuan, M.; Chen, C.; Wang, L.; Tang, Z.; Fan, Y.; Liu, X.; Ma, Y. J.; Gan, Y. Berberine-Loaded Thiolated Pluronic F127 Polymeric Micelles for Improving Skin Permeation and Retention. *Int. J. Nanomed.* **2020**, *15*, 9987−10005.
(56) Soares, J. P.; Santos, J. E.; Chierice, G. O.; Cavalheiro, E. T. G. Thermal behavior of alginic acid and its sodium salt. *Ecletica Quim.* **2004**, *29*, 57−64.
(57) Szekalska, M.; Sosnowska, K.; Zakrzeska, A.; Kasacka, I.; Lewandowska, A.; Winnicka, K. The Influence of Chitosan Cross-linking on the Properties of Alginate Microparticles with Metformin Hydrochloride—In Vitro and In Vivo Evaluation. *Molecules* **2017**, *22*, 182.
(58) Zhang, X.; Miao, F.; Niu, L.; Wei, Y.; Hu, Y.; Lian, X.; Zhao, L.; Chen, W.; Huang, D. Berberine carried gelatin/sodium alginate hydrogels with antibacterial and EDTA-induced detachment performances. *Int. J. Biol. Macromol.* **2021**, *181*, 1039−1046.
(59) Xue, M.; Yang, M.-X.; Zhang, W.; Li, X. M.; Gao, D. H.; Ou, Z. M.; Li, Z. P.; Liu, S. H.; Li, X. J.; Yang, S. Y. Characterization, pharmacokinetics, and hypoglycemic effect of berberine loaded solid lipid nanoparticles. *Int. J. Nanomed.* **2013**, *8*, 4677−4687.
(60) Bhanumathi, R.; Manivannan, M.; Thangaraj, R.; Kannan, S. Drug-Carrying Capacity and Anticancer Effect of the Folic Acid- and Berberine-Loaded Silver Nanomaterial to Regulate the AKT-ERK Pathway in Breast Cancer. *ACS Omega* **2018**, *3*, 8317−8328.
(61) Wang, Y.; Wen, B.; Yu, H.; Ding, D.; Zhang, J.; Zhang, Y.; Zhao, L.; Zhang, W. Berberine Hydrochloride-Loaded Chitosan Nanoparticles Effectively Targets and Suppresses Human Nasopharyngeal Carcinoma. *J. Biomed. Nanotechnol.* **2018**, *14*, 1486−1495.
(62) Kohli, K.; Mujtaba, A.; Malik, R.; Amin, S.; Alam, M. S.; Ali, A.; Barkat, M. A.; Ansari, M. J. Development of Natural Polysaccharide−Based Nanoparticles of Berberine to Enhance Oral Bioavailability: Formulation, Optimization, Ex Vivo, and In Vivo Assessment. *Polymers* **2021**, *13*, 3833.
(63) Chang, S.; Qin, D.; Yan, R.; Zhang, M.; Sui, B.; Xu, H.; Zheng, Z.; Hou, X.; Wang, Y.; Qi, C. Temperature and pH Dual Responsive Nanogels of Modified Sodium Alginate and NIPAM for Berberine Loading and Release. *ACS Omega* **2021**, *6*, 1119−1128.
(64) Sorasitthiyanukarn, F. N.; Muangnoi, C.; Ratnatilaka Na Bhuket, P.; Rojsitthisak, P.; Rojsitthisak, P. Chitosan/alginate nanoparticles as a promising approach for oral delivery of curcumin diglutaric acid for cancer treatment. *Mater. Sci. Eng., C* **2018**, *93*, 178−190.
(65) Li, L.; Li, J.; Si, S.; Wang, L.; Shi, C.; Sun, Y.; Liang, Z.; Mao, S. Effect of formulation variables on in vitro release of a water-soluble drug from chitosan−sodium alginate matrix tablets. *Asian J. Pharm. Sci.* **2015**, *10*, 314−321.
(66) Thai, H.; Nguyen, C. T.; Thach, L. T.; Tran, M. T.; Mai, H. D.; Nguyen, T. T. T.; Le, G. D.; Can, M. V.; Tran, L. D.; Bach, G. L.; Ramadass, K.; Sathish, C. I.; Van Le, Q. Characterization of chitosan/alginate/lovastatin nanoparticles and investigation of their toxic effects in vitro and in vivo. *Sci. Rep.* **2020**, *10*, 909.
(67) Chiu, C. F.; Fu, R. H.; Hsu, S. H.; Yu, Y. H. A.; Yang, S. F.; Tsao, T. C.; Chang, K. B.; Yeh, C. A.; Tang, C. M.; Huang, S. C.; Hung, H. S. Delivery Capacity and Anticancer Ability of the Berberine-Loaded Gold Nanoparticles to Promote the Apoptosis Effect in Breast Cancer. *Cancers (Basel)* **2021**, *13*, 5317.
(68) Sefidabi, R.; Mortazavi, P.; Hosseini, S. Antiproliferative effect of berberine on canine mammary gland cancer cell culture. *Biomed. Rep.* **2017**, *6*, 95−98.
(69) Akhter, M. H.; Rizwanullah, M.; Ahmad, J.; Amin, S.; Ahmad, M. Z.; Minhaj, M. A.; Mujtaba, M. A.; Ali, J. Molecular Targets and Nanoparticulate Systems Designed for the Improved Therapeutic Intervention in Glioblastoma Multiforme. *Drug Res. (Stuttgart, Ger.)* **2021**, *71*, 122−137.
(70) Ghaffarzadegan, R.; Khoee, S.; Rezazadeh, S. Fabrication, characterization and optimization of berberine-loaded PLA nanoparticles using coaxial electrospray for sustained drug release. *Daru* **2020**, *28*, 237−252.
(71) Rahman, M. M.; Islam, M. B.; Biswas, M.; Khurshid Alam, A. H. In vitro antioxidant and free radical scavenging activity of different parts of Tabebuia pallida growing in Bangladesh. *BMC Res. Notes* **2015**, *8*, 621.
(72) Hoshyar, R.; Mahboob, Z.; Zarban, A. The antioxidant and chemical properties of Berberis vulgaris and its cytotoxic effect on human breast carcinoma cells. *Cytotechnology* **2016**, *68*, 1207−1213.
(73) Farheen, M.; Akhter, M. H.; Chitme, H.; Akhter, M. S.; Tabassum, F.; Jaremko, M.; Emwas, A.-H. Harnessing Folate-Functionalized Nasal Delivery of Dox−Erlo-Loaded Biopolymeric Nanoparticles in Cancer Treatment: Development, Optimization, Characterization, and Biodistribution Analysis. *Pharmaceuticals* **2023**, *16*, 207.
(74) Yu, F.; Ao, M.; Zheng, X.; Li, N.; Xia, J.; Li, Y.; Li, D.; Hou, Z.; Qi, Z.; Chen, X. D. PEG−lipid−PLGA hybrid nanoparticles loaded with berberine−phospholipid complex to facilitate the oral delivery efficiency. *Drug Delivery* **2017**, *24*, 825−833.
(75) Feng, X.; Wang, K.; Cao, S.; Ding, L.; Qiu, F. Pharmacokinetics and Excretion of Berberine and Its Nine Metabolites in Rats. *Front. Pharmacol.* **2021**, *11*, 594852.

https://doi.org/10.1021/acsomega.3c01153
ACS Omega 2023, 8, 38806−38821